Ricardo Xavier da Graça Ferreira

Modulação acústo-ótica em fibra ótica para aplicação em sensores

Acoustic optical modulation in optical fibre for sensing applications

Dissertação apresentada à Universidade de Aveiro para cumprimento dos requisitos necessários à obtenção do grau de Mestre em Engenharia Física, realizada sob a orientação científica da Doutora Lúcia Bilro, bolseira de investigação em pós-doutoramento do Instituto de Telecomunicações e co-orientação científica do Doutor Rogério Nogueira, Investigador Auxiliar do Instituto de Telecomunicações.

o júri

presidente

João Filipe Calapez de Albuquerque Veloso, PhD
Professor Auxiliar,
Departamento de Física, Universidade do Aveiro.

Orlando José dos Reis Frazão, PhD
Professor Auxiliar Convidado,
INESC Tecnologia e Ciência e Astronomia, Departamento de Física, Faculdade de Ciências, Universidade do Porto

Lúcia Maria Botas Bilro, PhD
Investigadora Post-Doc,
Instituto de Telecomunicações.

Rogério Nunes Nogueira, PhD
Investigador Auxiliar,
Instituto de Telecomunicações.

acknowledgements

I would like to say my personal regards you to everyone directly involved in this project: Lúcia Bilro, Rogério Nogueira, Carlos Marques, Ricardo Oliveira, Nélia Alberto, João Prata from Instituto de Telecomunicações. My family for the support, understanding and believe until the end. For the future, I want to commit myself to make the most from the efforts of everyone who's supported me through this race against time. To everyone above, my personal thank you.

내 여자 친구 남 현수에게

palavras-chave

ótica, fibra ótica, sensor de fibra ótica, sensor intrínseco, sensor, viscosidade, índice de refracção, acústo-ótico, rede de Bragg

resumo

O presente trabalho teve como objetivo desenvolver um sensor de fibra óptica intrínseco para viscosidade com base no efeito acústo-ótico aplicado em redes de Bragg. Foram utilizadas fibras de silica e poliméricas para medições com baseadas no espectro e no tempo de resposta da rede quanto sujeitas ao efeito acústo-ótico. O resultado é um viscosímetro multi-paramétrico com um distinto potencial futuro. Com base no conhecimento adquirido, é proposto um novo design e mecanismo de detecção.

keywords optics, optical fibre, fibre sensor, intrinsic sensor, sensor, viscosity, refractive index, acousto-optic, Bragg grating

abstract The present work aimed to develop an intrinsic optical fibre sensor for viscosity based on the acousto-optic effect applied into fibre Bragg grating. Polymer and silica optical fibres were employed for measurements based on the spectra and the grating response times when subjected to the acousto-optic effect. The results is a multi-parameter viscometer with a distinctive future potential. Based on the knowledge acquired, a new design and sensing mechanism is advanced.

Contents

Acronyms

RI refractive index

FBG fibre Bragg grating

mPOF microstructured plastic optical fibre

POF plastic optical fibre

PMMA poly(methyl acrylate)

PCF photonic-crystal fibre

LPG long period grating

AOM acousto-optic modulation

PZT piezoelectric disc

EDFA erbium doped fibre amplifier

ECL external cavity laser

UV ultra violet radiation

dB decibel

dBm decibel referenced to one milliwatt

SNR Signal-to-Noise Ratio

PC physical contact

APC angled physical contact

Symbols

$\lambda_{\mathbf{B}}$ Bragg wavelength

$\lambda_{\mathbf{peak}}$ central peak wavelength

$\lambda_{\mathbf{laser}}$ laser emission wavelength

$\lambda_{\mathbf{a}}$ acoustic wavelength

$\mathbf{f_a}$ acoustic frequency

$\varnothing$ diameter

α attenuation

$\mathbf{\Lambda}$ grating period

$\lambda_{\mathbf{PM}}$ phase mask period

$\mathbf{n_{eff}}$ effective refractive index

$\mathbf{\bar{n}_{eff}}$ mean effective refractive index

$\mathbf{n_{AC}}$ alternating refractive index

$\mathbf{n_{AC}}$ direct refractive index

σ viscous stress tensor

η coefficient of shear viscosity

$\mathbf{P_{out}}$ output power

$\mathbf{t_{exp.}}$ exposure time

$\mathbf{Pulse_{freq.}}$ pulse frequency

$\mathbf{K}$ optical wavenumber

$\mathbf{K_a}$ acustic wavenumber

Chapter 1

Introduction

1.1 Motivation

The acousto-optic effect is already a well know effect but with only a few numerable applications, such as light modulation and deflectors [1]. However, some interesting new applications have been squeezing around the scientific community such as optical sensing. Previous simulations have demonstrated the main operation principle of acousto-optic modulation on optic fibre for viscosity sensing, with experimental validation on silica gratings [2–5].

These category of devices are very interesting for medical and scientific where high sensitivity is required [6, 7]. This work enhances the focus for in-situ real time monitoring for processing industries such as chemical, pharmaceutical, bioengineering, food, etc, that commonly use single sample analysis with delayed results. Just recently in the BioPIC'13 conference, photoacoustic systems revealed popular due the high-impact on discovery and treatment of biological problems [8].

In this work, acknowledging what is behind, tries to go further with experimental measurements, exploring a wider set parameters which would enable more advanced solutions for future viscometers. In sensing, *what to measure* versus *how to do it*, is the paradigm that requires an equilibrium between science and engineering.

1.2 Objectives

Develop, characterise and calibrate a prototype viscometer based on the acousto-optic modulation (AOM) of fibre Bragg gratings (FBGs) on an microstructured plastic optical fibre (mPOF). Explore the possibilities for integration and a commercial device.

1.3 State Of The Art

1.3.1 Sensing

Sensors are part of our everyday life as well as objects of research of the today's cutting-edge science. When a sensor is related with an energy conversion is also known as transducer. Being able to convert the measured information into an electric signal makes the sensor a commonly used device.

A sensor is a gauge that gives a response to a physical stimulation with the minimal impact on the quantity to be measured. A physical quantity can be measured directly or indirectly. Directly means that the response of the changing quantity is the raw value presented. Indirectly means that the value presented is related with the quantity to be measured. Nowadays most sensors operate in an indirect form. This method is only reliable with a fine calibration, which defines the range and operation conditions, sensitivity, accuracy and resolution. The operating range is a finite domain on which the gauge presents the desired sensitivity. The operation conditions are a defined set of external properties where the gauge can accurately measure the desired quantity such as: temperature, relative humidity, pressure, vibrations, strain, mechanical stability, etc. Resolution is physical limit to discern two different values e.g. the minimum value of δx detected by the sensor. Sensitivity of a gauge is the output response for a given change on the quantity to be measured e.g. the slope $^{\delta y}/_{\delta x}$, whereas accuracy is the degree of closeness of a measured quantity to the real value. Sensitivity and operating range are usually physically connected, where in order to get higher sensitivity on a quantity, the operating range will get shorter or vice versa. Finally, a sensor should be reliable, giving the same response or value for any repeated measurement.

1.3.2 Optical Fibre Sensing

The advent of optical fibre sensing arrived as an application of the optical fibres, firstly suggested in 1966 by Kao and Hockham in [9], and introduced in 1967 by Menadier and Kissenger in [10]. Their major advantages over the classical transducer sensor are: greater sensitivity, reduced size and weight, higher reliability and electromagnetic immunity [11]. Through the years, commercial and scientific fibre optic sensors have been developed and deployed combining this advantages with the measurable phenomena [12]. Despite the major advances, the basic principle of optical fibre sensor still remains to be the detection of the radiation interaction with physical phenomena.

The fibre optic based sensors had suffer major evolutions, closely related with the propose of their application and sensing mechanism [1, 11, 12]. There are two main types of fibre sensors, extrinsic and intrinsic. Extrinsic sensors are the ones who interrogate the medium, detecting changes in light properties due to the medium. Whereas in intrinsic sensors the medium affects directly the guidance of light inside the fibre [13]. As illustrated with in Fig. 1.1 (a), generally optical fibres are produced with a core region covered with a cladding layer. For step index fibres materials for the core and cladding are chosen in

order to produce a refractive index (RI) step on the interface between the two. For a given radiation wavelength, the RI difference defines a critical angle above which, with respect to the normal to fibre axis, all the radiation is reflected leading to total internal reflection.

The main materials used to produce optical fibres are silica and poly(methyl acrylate) (PMMA). Silica is the standard for sensing and optical telecommunications [12]. The PMMA based fibres, also known as plastic optical fibre (POF) promise a intrinsic sensing advantages, easier to handle and more flexible. However the technology behind PMMA is still in its early stages of development, which is reflected on high attenuation coefficient of $\alpha =\sim 100\, dB/m$ at $1590\, nm$ for a common single mode fibre [14].

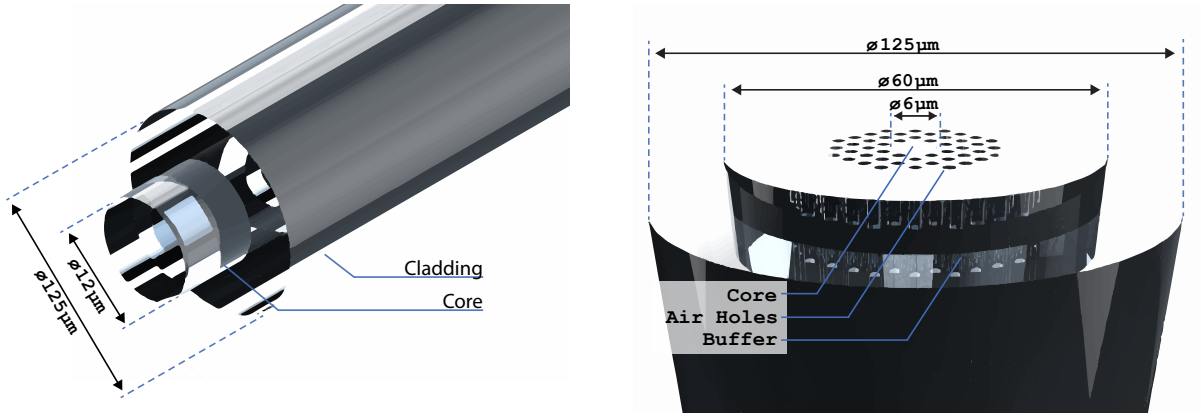

(a) (b)

Figure 1.1: Rendering of a single mode fibre (a) and (b) a microstructured fibre with a core surrounded by air holes which act as modified form of total internal reflection. The same material extends wider than in the single mode fibres with the typical diameters indicated. The relative dimensions are exaggerated for illustration purposes.

Fig. 1.1 illustrates the (a) single mode fibre where the RI change between the core and cladding are responsible for the full internal reflection. Whereas in (b) an mPOF is presented made by one solid material, where the light guidance is achieved through a circular array of air holes around the core. These holes run along the entire length of the fibre wrapping the core with a lower RI.

In silica fibres these structures are known as photonic-crystal fibre (PCF). Pioneered in 1996 by Phillips Russell at the University of Southampton [15], PCFs they are indeed very difficult and expensive to produce. Later the University of Sidney, presented a low cost solution based on PMMA known as mPOF [16,17]. These fibres can achieve $\alpha = 0.192 dB/m$, highly capable to accept dopants due to the PMMA acceptability and easy access through the holes [18]. The propagation of light on mPOFs is far more complex than on the common fibres and is not covered in this work. They do provide lower cost for single mode fibres while enhancing the sensing properties [17, 18].

Photonic structures can be inscribed within the core, the most common is known as FBG. Gratings are a periodic modulation of local the RI with lengths of a few millimetres.

An FBG is illustrated in Fig. 1.2 (b), as whole it behaves as Bragg reflector, which for certain wavelengths, satisfy the Eq. 1.1. This selective wavelength, known as the Bragg wavelength (λ_B), is dependent on the effective RI, $\overline{n}_{eff}$ and the grating period (Λ) [19].

$$\lambda_B = 2\,\overline{n}_{eff}\,\Lambda \tag{1.1}$$

The inscription of Fibre Bragg Gratings can be made by two main processes: the two beam interference or phase mask diffraction to achieve a spatial modulation of the wavefronts. The phase mask process is the standard for telecommunications, as it is easier and more reliable to reproduce high quality gratings [19]. As we look to Eq. 1.1, the second term is dependent on the grating period Λ. Thus it is also dependent on the inscription process, which for a phase mask process comes as $\Lambda = {}^{\Lambda_{PM}}/_{2}$ [20].

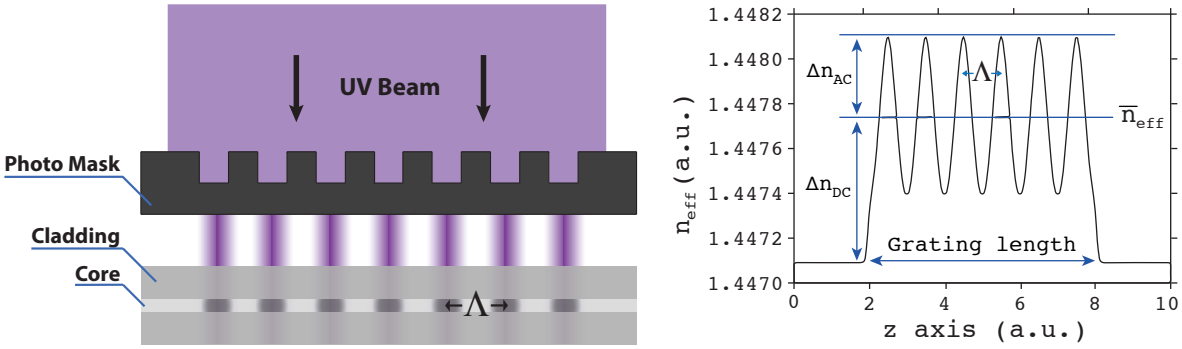

(a) (b)

Figure 1.2: In (a) the illustration of the FBG inscription by the zero order phase mask diffraction and (b) periodic modulation of the effective RI (n_{eff}). The phase mask period (Λ_{PM}) creates fringes of UV resulted by the zero order beam diffraction.

A general inscription of the index modulation of FBG is illustrated in Fig. 1.2 (a). The incidence of a UV coherent laser beam on the phase mask creates a patterned profile, corresponding to fringes of constructive and destructive phase interference. The fringes separation are defined by the phase mask period, Λ_{PM}, inscribing the pattern via photo-polymerisation of the core. Each fringe defines an effective RI separated by period $\Lambda = {}^{\Lambda_{PM}}/_{2}$ [19]. For silica fibres the photosensitivity is achieved via doping, although for POF it is not compulsory to be doped, being the theory behind the non doped POF inscription phenomena not yet completely defined [21].

1.3.3 Acousto-Optic Effect

Predicted by Brillouin [22] and confirmed by Debye & Sears [23], the acousto-optic effect was consolidated by the end of 1930s [1, 24]. Back in 1995 Cornell *et al.* achieved the Bose-Einstein condensation on which they applied AOM as light deflection mechanism, later receiving the Noble Prize of Physics in 2001 [25]. Besides the nobel scientific applications,

the AOM has been employed on events that generate acoustic emissions such as: materials deformation and degradation, industrial solids fabrication and fluids flow processes, friction, thermal and phase transformations [1, 26].

The basic idea is the following: the passage of an acoustic wave through a material excites periodic variations of stress, which, through the photoelastic effect, cause modifications of the RI, which in turn influences the propagation of light waves [1].

The photoelastic effect is the optical response to the applied stress or local pressure, commonly used with materials that exhibit the property of birefringence. Using acoustical waves through the photoelastic effect, it is possible to modulate the local RI, δn_0, which in turn creates a grating capable of deflecting certain optical frequencies, as illustrated in Fig. 1.3.

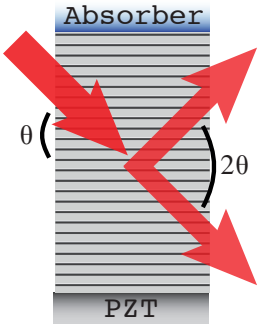

Figure 1.3: Illustration of the AOM where the acoustic plane waves, through Bragg diffraction, behave as filter for a certain wavelength.

This grating is formed only by the acoustic wavefronts, working as a Bragg diffraction mechanism for $Q \gg 1$ [1].

$$Q = \frac{K_a^2 L}{n\, K}, \tag{1.2}$$

where K_a is the acoustic wavenumber, L is the width of the slab from Fig. 1.3 (a), n is the medium RI (isotropic) and K is the optical wavenumber.

From Eq. 1.2, it becomes clear that for proper operation, the mechanism is limited by acoustic frequency, which is usually low with respect to the optical one. For acoustic frequencies $f^* < 500MHz$, the Bragg angle comes $\theta \approx 1°$ [1]. The system can be optically explored to generate radiation refraction, diffraction, and beam interference effects. The nature of the effect is such that it can be used on the optical side e.g. modulate, deflect or filter certain radiation wavelengths, but also on the acoustic side e.g. use the optical beam to detect properties of ultra-sonic waves [1, 26].

1.3.4 AOM & fibre optics

As described in detail by Oliveira *et al.* and Marques *et al.* in [2] and [27], acoustical modes create a perturbation on FBGs. A standing acoustical wave coupled into a optical

fibre with an FBG has the ability to change the optical properties of the structure. The strain field changes the local RI via photoelastic effect. If the longitudinal acoustical wavelength is longer than the FBG length, the strain generates a local RI modulation of the FBG, causing a chirp on the grating as seen in Fig. 1.4 (a). For a transversal or flexural wave whose wavelength is longer then the FBG length, the microbendings on the fibre attenuate the FBG reflectivity due to a loss on the phase matching condition, as seen in 1.4 (b). In addition, flexural waves create orthogonal displacement of fibre with respect to its axis, therefore vertical compression and rarefaction zones appear. If acoustic wavelength is longer then the length of the FBG, multiple compression and rarefaction create a greater decrease of the FBG reflectivity [5].

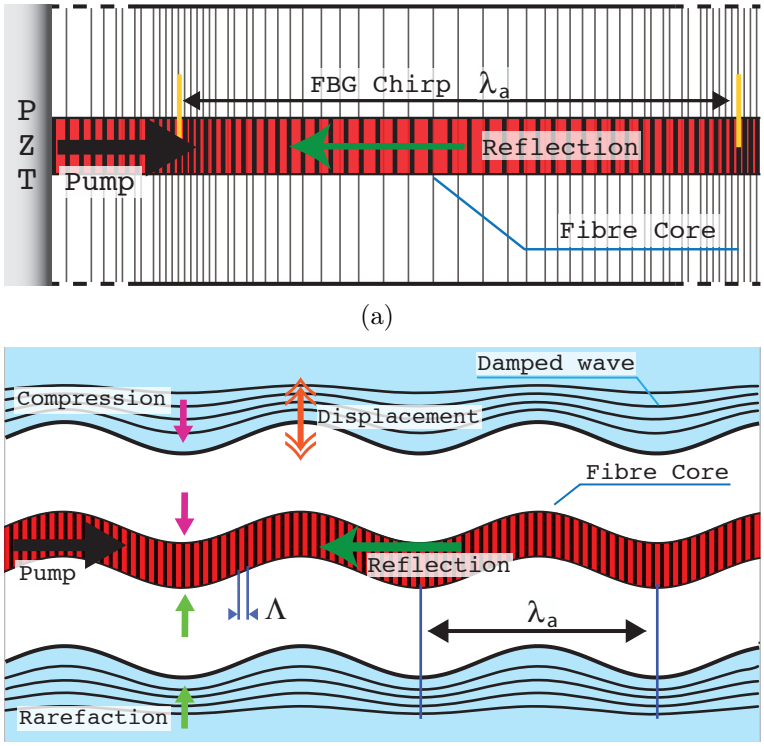

Figure 1.4: Illustration of two main applications of the AOM in fibre optics. In (a) the interaction of a longitudinal acoustic wave with an FBG causing a chirp, in (b) interaction of a flexural wave with an FBG causing bends on the fibre with compression and distension zones. The λ_a represents the acoustic wavelength and Λ the grating period.

Optical fibres are flexible and present a small diameters $(100 - 250\,\mu m)$, therefore a horn is required to couple the acoustical waves into the fibre. A silica horn was developed by Oliveira *et al.* in [2]. Simulations have optimised the shape, length and diameters to achieve efficient transfer of the acoustical load into the fibre as well as conversion of longitudinal waves into transverse waves [2, 28–31]. The acoustical modes were obtained by Marques *et al.* via the finite element method [32], as seen in Fig. 1.5. Simulations predict strong

flexural modes bellow the 400 KHz regime with and longitudinal modes predominant for higher frequencies [29, 31]. Hybrid modes also exist being the flexural component dominant for lower frequency regime.

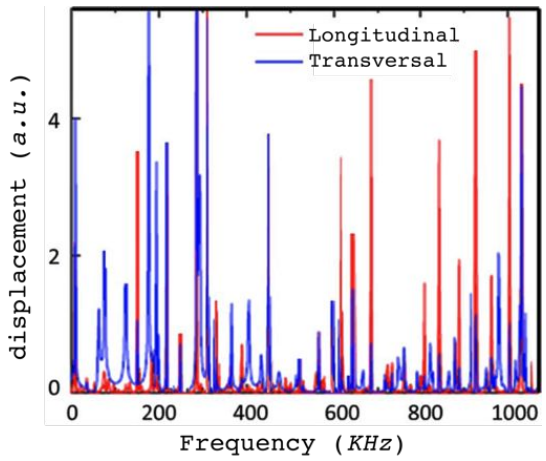

Figure 1.5: Simulation results for Longitudinal and Transverse modes frequencies adapted from [32].

The theory behind the system is divided in the following order: generation of acoustical waves, coupling of modes on the fibre and acousto-optic interaction with the inscribed grating. Simulations cover a wide range of parameters relating the horn shape and dimensions, strain, longitudinal and transverse acoustic resonant modes and optical properties of the fibre grating. The control over optical properties of the fibre through the AOM enables applications such as: fast tunable optical notch filters, power control for Q-switched lasers, writing gratings under acoustic excitation and sensors for biomedical, structural health monitoring [3, 11, 27, 28, 30]. Viscosity sensing comes as an interesting application of AOM in fibre optics as reviewed by Pohl *et al.* in [28].

1.3.5 Viscosity Sensing

Viscosity of a fluid is a measure of its internal resistance to flow [33]. In fact, viscosity is net result from the shear stress friction between the layers of a fluid that are moving at different velocities. In fluid mechanics is defined by the viscous stress tensor of Eq. 1.3 [33]. It is a measure of how a point within the fluid subjected to a strain rate, will experience an internal stress due to the friction between the moving layers of the fluid. When this internal stress is linear with the strain rate, the fluid is called $Newtonian$, other cases are know as $non - Newtonian$ [33, 34]. Newton's law for the shear stress viscosity is expressed for the general case as:

$$\sigma_{xy}(y) = \eta \frac{\delta v_x(y)}{\delta y}, \tag{1.3}$$

where σ_{xy} is the viscous stress tensor, η is the coefficient of shear viscosity and ${}^{\delta v_x}/_{\delta y}$ is the local shear velocity.

For isotropic Newtonian fluids i.e. stress tensor independent of the flow stress state and velocity, the planar viscous friction or drag force, comes as:

$$D \approx -\sigma_{xy}\, A = -\eta\, \frac{vA}{d}, \tag{1.4}$$

where D is the drag force, η the shear viscosity, d the thickness of each layer of the fluid at the velocity v with a contact area A.

From general case of Eq. 1.3, can be obtained the general solution of the simplified Navier-Stokes equation for the velocity-driven planar flow that relates force with viscosity, presented in Eq. 1.4 [33]. It represents the force needed to move a thin layer of a fluid with viscosity η on a surface with a velocity v, subjected to dimensionality constrains. Adapting the terms of Eq. 1.4 for different shapes and sizes, viscometers can be build, measuring damping of momenta, e.g. falling ball, falling piston, disc rotation and piston vibration. Using the tube flow solution for the Eq. 1.3, rheometers can be built, measuring the flow of a fluid through a cross-section. Rheometers are gauges for fluids which viscosities vary with the flow conditions, i.e. fluids that cannot be described by only one value of viscosity, usually for the study of materials with both solid and fluid characteristics. Thus, a viscometer is a gauge that only measures viscosity on the laminar flow condition, namely aqueous based fluids. The current commercial viscometers and rheometers typically present a wide operating range from 15 up to $320 \times 10^6\, mPa \cdot s$ depending of the model, configuration, accessories and type of fluid [35]. Their features are dependent on a few interchangeable parts separately priced. New advances such as the Electromagnetically Spinning Sphere Viscometer (EMS Viscometer), developed by Sakai *et al.* at the University of Tokyo, present a device capable of viscosity measurements as low as $1.0\, mPa \cdot s$ [7].

Regardless the origin, these are table devices for a single sample at a time. This implies that for any continuos processes, a sample has to be taken and analysed off-line. They are based on a classical operating principle which measures torque or power, frequency or time and the velocity of mechanical parts which present a limitation to resolution. Both scientific devices and commercial manufactures do not present the actual viscosity resolution, instead they present resolution of the active mechanical instrumentation.

Due to the above limitations and scarce of flexible instruments, the need for acousto-optic viscometer becomes plain. It does have the potential for higher resolution, more flexibility and also integration to fit on in-situ monitoring systems. In previous works, Oliveira *et al.* demonstrated AOM of silica FBGs and long period gratings (LPGs) for viscosity sensing [3,4]. Inscribing FBGs on silica fibres is a well optimised process and nowadays one can easily get a stable $20\, dB$ reflection peak with a baseline $> -35\, dBm$ [5, 27]. FBG inscription on POF is well know for their higher sensitivity to strain and temperature, usually present resolution two to three orders of magnitude higher in comparison to silica [12]. In addition, polymers present a impedance close to the water allowing uniform acoustic frequency response [36], in particular mPOFs present higher sensibility to aqueous sensing [18]. Although technology behind FBG inscription mPOF is still in their early stages presenting high attenuation

($\alpha_{847.6nm} = 10\,dB/m$), low reflectivity ($-61\,dBm$) and broaden spectrum ($> 0.29\,nm$) [37].

A possible sensing principle to measure viscosity with AOM on a FBG is to associate the damping of a flexural wave on the fluid with a change in the perturbed FBG. Higher viscosities reduce the displacement of flexural modes reducing the perturbation on the grating. The amplitude of the flexural mode is associated with a stress tensor which depends on viscosity. In this mechanism, illustrated in Fig. 1.4 (b), as the mode resonates surges compression on the top and distention on the bottom, modulating the RI of the grating via photoelastic effect [1, 5].

Chapter 2

Instrumentation

2.1 Principle Of Operation

The whole sensor was projected to reflect the sensing mechanism, as seen in Fig. 2.1. It can be structured in the following order: the piezoelectric disc (PZT) generates longitudinal acoustic modes, which are converted to a flexural modes by the horn. The flexural modes on the fibre create microbends on the grating. The bends provoke compression and rarefaction zones, modulating and pertubating the FBG reflectivity [5, 27, 32]. As the amplitude of displacement depends on the immersed fluid's viscosity, an increase on viscosity forces a decrease of the displacement and in turn perturbation effects decrease [2, 28, 33, 34].

2.2 Sensor Design

An isometric view of the assembled sensor is presented in Fig. 2.1 (a), with a cross-section view of the main operating components presented in Fig. 2.1 (b). For each part of the assembly there are associated features, the assembly is discretised and described as follows:

Supports

A steel pillar with two additional aluminium bodies are responsible for positioning the sensor in an open vertical space. They feature angular and vertical adjustments. As shown in the photograph, Fig. 2.2 (a), a micrometer is added for vertical precision control, allowing fine tune of the applied strain into the fibre after glued.

PZT & Horn

Placing the PZT operation axis perpendicular to the support bodies avoids the reflection of the acoustic waves on the joints. As presented in Fig. 2.1 (b), the aluminium body, the PZT and the horn are all glued together with concentric holes, however, the horn diameter is smaller than the back hole drilled in the aluminium body that supports it, thus, avoiding acoustic noise generated in the glued PZT slab. The PZT can generate signals for frequencies up to 1 MHz. The horn is made

from a silica glass, it is responsible for the conversion of longitudinal modes into flexural modes, coupling the acoustic load from a larger diameter (PZT base) into the fibre. From the available horns, the best match is a compromise between the ideal shape, the correct size and internal hole diameter to fast the fibre. The final dimensions of the horn used are: $\varnothing_{base} \approx 8\,mm$, $\varnothing_{tip} \approx 2.5\,mm$, $\varnothing_{internal} \approx 125\,\mu m$ and $length = 38.4\,mm$.

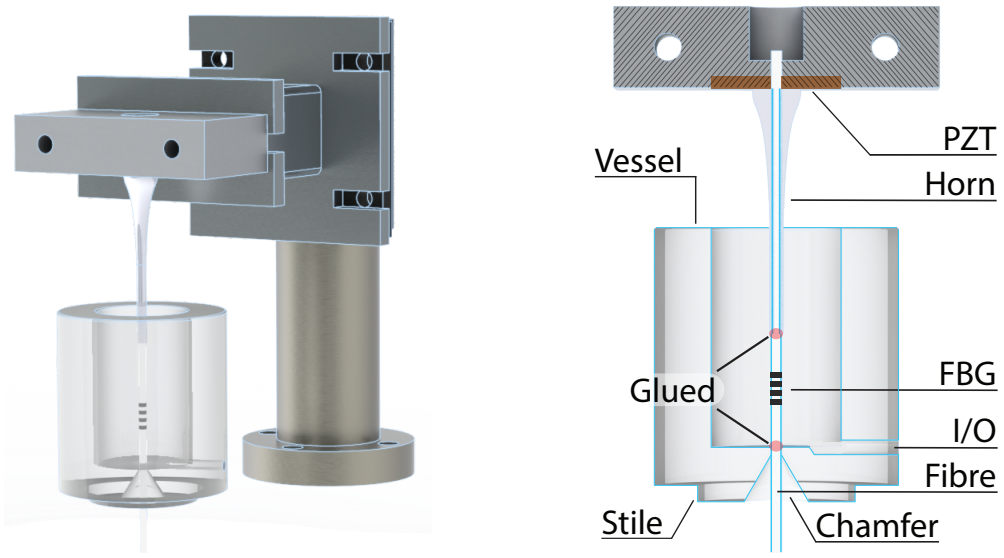

(a) (b)

Figure 2.1: Rendering of the projected parts for the final assembly in (a). In (b) a cross section rendering showing the detail of the PZT disc assembled inside the aluminium block, the typical shape of the glass horn glued to the PZT and the FBG centred between the horn and vessel. Fibre diameter and vessel's transparency are adjusted illustration purposes.

Vessel

The vessel was designed to hold the fluid and glue the fibre, machined from a solid nylon rod into the final tube shape assuring a precise dimensionality. It features a side hole to allow an easy input and output of the fluid samples; on the bottom there is a circular chamfer creating a conic puncture, allowing spacious access to place fibres; and finally a circular stile allows the vessel to be fasten on a steel tube, as seen in Fig. 2.2 (a).

Fibres

The fibre is placed vertically through the horn concentrically with the vessel's puncture, as seen in Fig. 2.1 (b). The FBG must remain centred between the glued points, the region of maximum acousto-optic interaction, with a minimum length of 3 cm

between the glued point and the FBG. Silica fibres are interrogated from the top and mPOF are interrogated from the bottom, placing the cure outside of the vessel within the chamfer region.

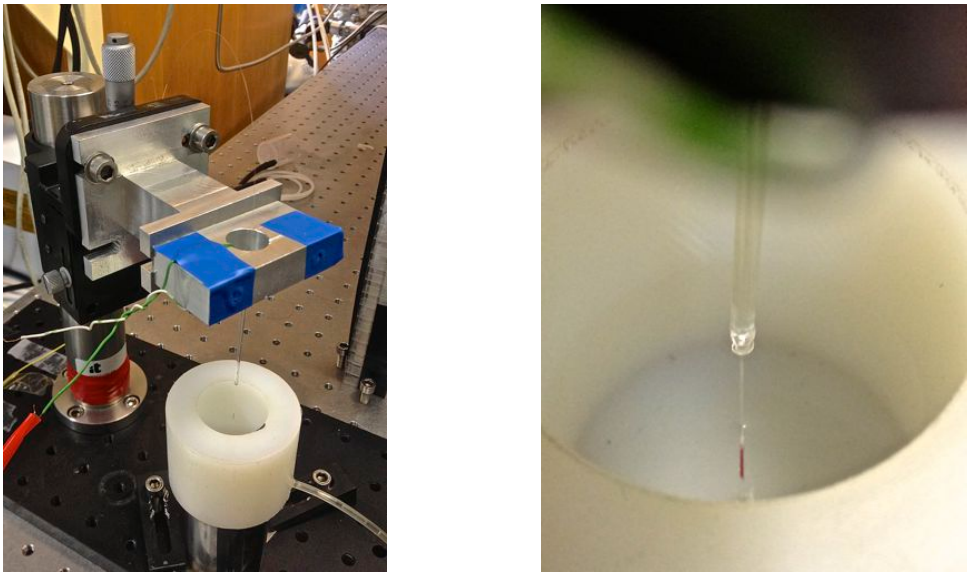

(a) (b)

Figure 2.2: Photographs of the assembled sensor. The photo (a) shows the whole sensor, interrogated with a silica fibre from the top, where a micrometer was added for strain control. The photo (b) shows a close up inside the vessel, the region for the liquid samples, where the FBG is marked in red on fibre.

The photograph from Fig. 2.2 (a) presents an outlook of the sensor. To ensure mechanical stability, the apparatus is fixed to an pneumatic optical table. The photograph from Fig. 2.2 (b) presents a closer view of the vessel interior, where the detail of fibre glued to the horn can be seen with the FBG marked in red.

2.3 Materials

In order to characterise the system for viscosity, ten calibration samples were made using D(+) - Glucose anhydrous ($C_6H_{12}O_6$) solutions. Table 2.1 presents the prepared samples mass, viscosity and the respective RI (n). D(+) - Glucose anhydrous is a standard calibration substance that presents quadratic and linear dependance with solute concentration for viscosity and RI respectively [38].

Table 2.1: Set of calibration samples based in $D(+) - Glucose$, where sample 0 corresponds to distilled water. Substance produced by Quimitécnica Lda. and data obtained through Hydrotechnik [39]. Values for a temperature of $25°C$.

Sample	Conc. (mol/L)	η $(mPa \cdot s)$	n
0	0.000	0.8940	1.3333
1	0.249	1.0837	1.3410
2	0.499	1.1496	1.3471
3	0.749	1.3079	1.3531
4	1.000	1.5600	1.3592
5	1.250	1.9038	1.3653
6	1.501	2.3419	1.3713
7	1.751	2.8711	1.3774
8	1.998	3.4847	1.3834
9	2.250	4.2038	1.3895
10	2.500	5.0100	1.3955

2.3.1 Fibres Details

The section presents the technical information of the fibres, their respective FBGs inscription using the phase mask method explained in section 1.3.2 and the fibre's connection system associated.

Silica

- Producer: Fibercore Ltd
- Fibre: Silica PS1250/1500 single mode doped with Boron, $\varnothing_{fibre} = 125\,\mu m$, $\varnothing_{core} = 8\,\mu m$, $\alpha_{1550nm} = 0.12\,dB/m$;
- FBG Phase Mask: $\Lambda_{PM} = 1073.11\,nm$, length $= 20\,mm$;
- Laser: Coherent BraggStar pulsed excimer KrF, $\lambda_{laser} = 248\,nm$, $P_{out} = 4\,mJ/pulse$, $Pulse_{freq.} = 100\,Hz$, $t_{exp.} = 25\,sec$;
- Splice: Fujikura Arc Fusion Splicing FSM-60S.

mPOF

- Producer: Kiriama Pty Ltd, Australia;
- Fibre: PMMA SM-125 single mode, $\varnothing_{fibre} = 125\,\mu m$, $\varnothing_{core} = 6\,\mu m$, $\alpha_{800nm} = 4.80\,dB/m$;
- FBG Phase Mask : $\Lambda_{PM} = 1048.70\,nm$, length $= 2\,mm$;
- Laser: Kimmon $HeCd$ CW, $\lambda_{laser} = 325\,nm$, $P_{out} = 30\,mW$, $t_{exp.} = 55\,min$;
- Splice: Photosensitive UV Cure with Norland Optical Adhesive 68 (> 3 layers), $\lambda_{laser} = 325\,nm$, $t_{exp.} \sim 30\,min$, $n_{cured} = 1.54$.

2.4 Methods

2.4.1 Fibres Connection

The fibres used for FBGs inscription present relatively high attenuation. A common procedure is to connect the grating fibre to a telecom fibre which presents $\alpha_{1550nm} = 0.02\,dB/km$ [12]. The procedure requires a 8° cleavage on the telecom fibre to eliminate backscatter before connecting the sensing fibre. Then the fibres' cores are aligned and spliced together. In silica fibres the alignment and splicing is automatically made by an arc fusion splicing equipment, resulting in a loss on the fibres' interfaces of $\sim 0.04\,dB$. However arc fusion splicing is not possible for plastics. The common technique to splice a POF into a telecom fibre is known as cure. A cure involves the use of a viscous optical adhesive to bond the two fibres via UV exposure. It also works as an RI adaptation between silica and PMMA.

The ideal situation for a cure is illustrated in Fig. 2.3 (a). It assumes a perfect cores' alignment of both fibres, a sharp cleavage of the faces and a uniform deposition of adhesive. The optical adhesive is added in a small drop to the fibres' faces, leant together and a few minutes of UV exposure dries the cure. This first layer ensures the optical splicing, further more layers are added to provide mechanical support to the splicing.

In fact the real case for a cure involves issues and imperfections as illustrated in Fig. 2.3 (b). Firstly the imperfections of the manual cleaving and alignments lead to an incorrect placement of the faces. The fibre is lay down on a plate and cut by razor blade both heated at $\sim 70°C$. A uniform cleaving temperature defines the optical quality of the face while a smooth incision ensures not plugging the holes microstructure.

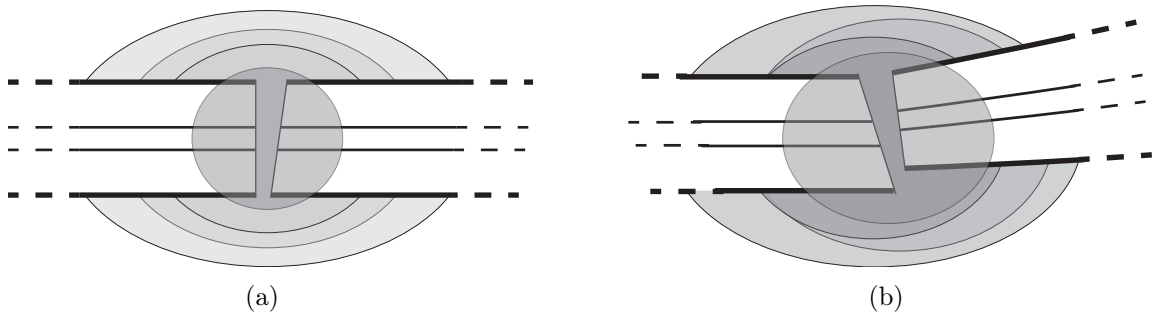

Figure 2.3: Illustration of the cure alignment and the adhesive is deposited in several layers, one at a time, until it reaches a stable joint. The optical adhesive also features a coupling of RI once it is cured. The ideal case is illustrated in (a) and a more real situation in (b) presenting common problems such as: stretched and cut-off the cross section faces.

Also as the cure dries the internal tensions of the adhesive tend to misalign the fibres leading to a cut-off the cross section faces. In addition, the cures' drops accumulate in the bottom due to gravity forming a bead, stretching the fibres.

Overall, these facts resulted in a loss on the interface of 3 to 7 dB. Besides, the cure is fragile and presents sensibility to any bend and strain.

2.4.2 Testing AOM

The active component driving the sensor is the PZT, electrically connected to a function generator (Tektronix AFG3101). It is responsible to generate the AC signals that resonates the acoustic waves, limited to a maximum output load of $20\,V$, the voltage used for all measurements.

The wave type can be determined by observing the variation of the FBG spectra with the coupling modes. Longitudinal modes exist for all frequency range, up to $1\,MHz$. They do a spectrum shaping as these modes generate local compressions, parallel to the grating, improving the phase match condition and cleaning the majority of thermal noise [40]. They do not exhibit an observable change to the height, bandwidth or peak position (λ_{peak}).

As for the flexural modes, the spectra always presents attenuation of the reflection peak. As the height of the peak drops, it also broadens due to a phase match modulation of the RI [3].

Fig. 2.4 presents the typical spectra of flexural modes for mPOF and silica's FBGs with the OFF and ON states represented blue and magenta lines respectively. Note that silica's reflectivity is fairly high with Signal-to-Noise Ratio (SNR) levels negligible when compared to mPOF. For the AOM both silica and mPOF present a very similar height decay of $\sim -3\,dB$.

In the case of silica's FBG, presented Fig. 2.4 (b). The bandwidth broadens significantly to ~ 3.5 times the initial width, clearly displayed in Fig. 2.5 (b) inset.

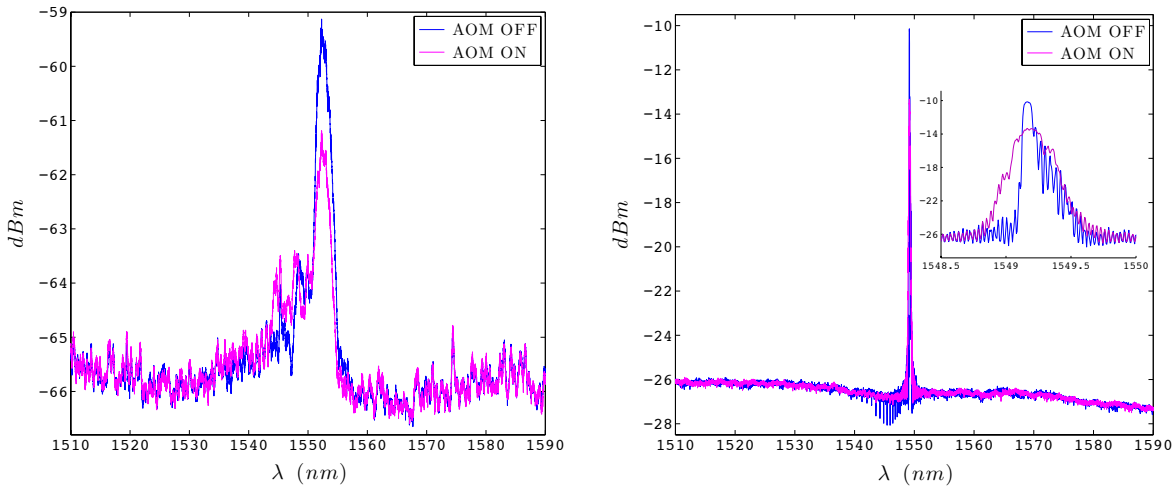

(a) (b)

Figure 2.4: Typical spectra of FBG reflection peak for (a) mPOF and (b) Silica for a distilled water sample. The blue and magenta spectra correspond to the AOM state OFF and ON respectively.

For a resonant mode, the interest is to monitor changes in the FBG reflection peak properties (central wavelength, height and bandwidth). As described, height and bandwidth

are dependent on AOM, but, the central wavelength of the peak (λ_{peak}) of the peak is affected as well. However, the FBGs are naturally capable of sensing temperature and strain, the typical sensitivities are: $\sim 10\,pm/°C$ and $\sim 1.15\,pm/\mu\epsilon$ for silica gratings, -50.1 to $-95\,pm/°C$ and $\sim 1.13\,pm/\mu m$ for POF gratings [14, 41]. In addition, PMMA is also known for moisture absorption and changing the reflection properties of FBG, which makes it sensible to RI of the water [18, 42, 43].

Two different types of measurements were taken: static and dynamic. Static measurements corresponds to a spectrum that is stable in time with AOM OFF and ON states, where in the dynamic the interest is to monitor the transition in between the states.

The schematic for static measurements is presented in Fig. 2.5 (a). The equipment *Micron Optics - Optical Sensing Interrogator SM125* was used to interrogate the FBGs, it operates in the range $1510 - 1590\,nm$ with a resolution of $5\,pm$, minimum power detection of $-80\,dBm$ with a fixed acquisition frequency of $2\,Hz$. To test a large number of conditions, hundreds of data files are generated. A $Matlab^{®}$ user interface was developed for fast data processing, as seen in Fig. 2.5 (b), presenting the typical spectra of a silica FBG under analysis. The developed software allows to easy and rapid analysis, comparison of spectra pairs and plot the results of a full measurements set. It features peak detection, bandwidth, height and area calculations, thus, it also provides information comparing and normalising the calculated values, adjusting spectra scales for a detailed viewing. The code is attached in section A.

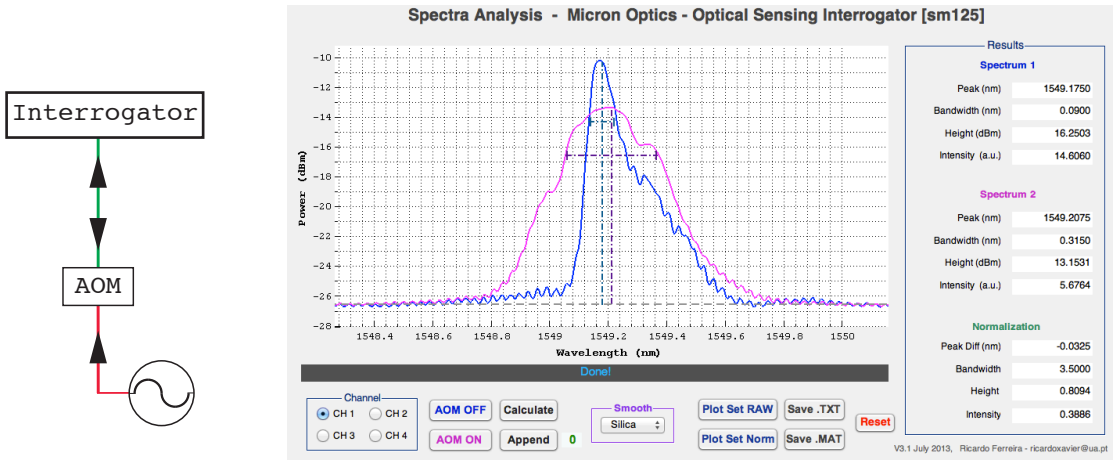

(a) (b)

Figure 2.5: Static measurements information with (a) the experimental apparatus, where the green and red lines correspond to optical and electric signals respectively. In (b) is presented the *Spectra Analysis* software developed in $Matlab^{®}$, presenting an example spectra of a silica FBG where the AOM OFF and ON correspond to blue and magenta lines respectively. Note that both power and wavelength scales are automatically scaled to the reflection peak region.

For dynamic measurements the apparatus presented in Fig. 2.6 (a) was used. The apparatus converts optical power into electrical signals to be further analysed in an oscilloscope.

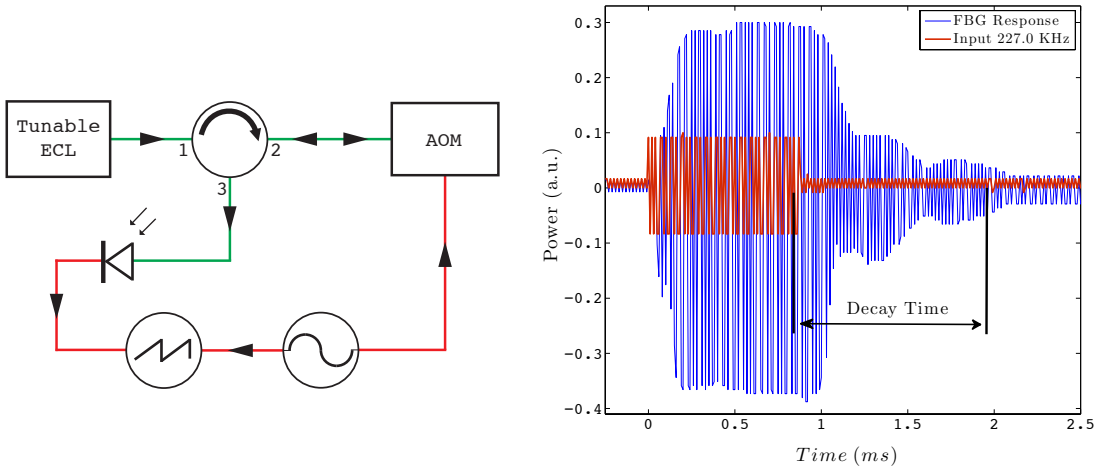

(a) (b)

Figure 2.6: Dynamic measurements information with (a) the experimental apparatus, where the green and red lines correspond to optical and electric signals respectively. In (b) an example of time response profile for a silica FBG on distilled water with the decay time is marked. Note that signal scales are adjusted for clear overview, as the input comes in V and the response in mV.

A tunable external cavity laser pumps at the central wavelength, the optical signal reflected is then converted into electrical signal. The response signal and the PZT excitation signal were observed on the oscilloscope. The complex impedance of the PZT disc implies that the rate of drained current from the function generator is not linear in the frequency space, also it is highly dependent on the load of the system where the PZT is integrated [44]. Initial test have demonstrated this inconsistency in the rising and stabilisation times. For this reason it was chosen the decay time, as seen in Fig. 2.6, has it does not depend on the PZT current consumption.

2.4.3 Procedure

The final apparatus consists of the sensor projected in Fig. 2.1 and 2.2, where a mPOF and silica fibres were assembled. For the silica fibre, as the fusion splicing keeps the same diameter, the fibre can be installed from the top, through the whole horn passing on the vessel's puncture and be glued in the correct points. For the mPOF fibre, the cure itself is a ball connecting both fibres, close to the FBG to avoid attenuation. Then it cannot pass through the horn and must be installed from the bottom, the fibre pass through the vessel's puncture into horn. The correct points are glued and the cure remains in the empty space on the bottom of the vessel, as detailed in Fig. 2.1 (b).

The vessel is filled with 16 ml of the sample to be tested using a syringe connected to a plastic tube into the vessel's side hole (I/O). Stabilisation time was 3 min. For static measurements the interrogation apparatus was used, as seen in Fig. 2.5 (a). An AOM OFF spectrum was taken immediately followed for a AOM ON spectrum, repeated for

all the interesting frequencies before changing samples. For dynamic measurements the fast measurements apparatus was used, as seen in Fig. 2.6 (a). The interrogator was used to tune the external cavity laser (ECL) to the exact position of λ_{peak}. For excitation of the modes the function generator was used in burst mode with a pulse duration and pulse interval of $500\,ms$. The exciting frequency and FBG response are displayed on the oscilloscope and single time profiles of the response were taken for each frequency of interest, as presented in Fig. 2.6 (b).

Chapter 3

Results

In order to find the frequencies for the modes of the system, a sweep was taken acknowledging the intrinsic longitudinal modes of the PZT. For viscosity the real interest are flexural and hybrid modes only. Tab. 3.1 presents all the modes found for both mPOF and silica fibres, which are not exactly the same as lower interaction ones were discarded. The modes of the system are very close to the ones predicted by Marques *et al.* in [32], in fact the 302.2 KHz flexural mode was especially referred as the highest one. Hybrid modes were identified by Oliveira *et al.* and Marques *et al.* and presented in Fig. 1.5 [2, 30, 31]. Although the design of the sensor in this work is adapted for viscosity measurements, the parameters of the AOM remain similar, therefore the modes appear in close frequencies to ones presented in the Fig. 1.5 from section 1.3.4.

Table 3.1: Coupling frequencies of AOM assembled system as presented in Fig. 2.1 and 2.2 with the respective mode.

Fibre	f_a (KHz)	Mode
mPOF	76.5	flexural
	203.7	flexural
	213.9	hybrid
	302.2	flexural
	400.0	hybrid
Silica	58.0	flexural
	86.4	flexural
	115.0	flexural
	221.7	flexural
	227.0	flexural

An overview of all the measured scenarios are summarised in Tab. 3.2. The 2^{nd} row (AOM OFF) correspondes to fibres characterisation and the 3^{nd} row (AOM ON) to static calibrations.

As referred in section 2.3 and presented in Tab. 2.1, glucose samples exhibit a quadratic

relation between viscosity and RI, affecting λ_{peak} of mPOF fibre. In order to characterise these fibres to RI for both silica and mPOF, rest state spectra were taken for all samples, as seen in Fig. 3.1. As the RI increases, in the mPOF's FBG the λ_{peak} does a blue shift, as for silica's FBG there is no significant variation. This result is expected due to moisture absorption characteristic of PMMA [18, 43], presenting the ability to discern RI.

Table 3.2: Summarised characterisation and calibrations achieved for mPOF and silica fibres with glucose samples.

	mPOF	Silica
AOM OFF	RI	RI
	water level	—
	water absorption	—
AOM ON	λ_{shift}	—
	$\Delta Band.$	$\Delta Band.$
	$\Delta Height$	—
Dynamic	—	decay time

3.1 Initial Characterisation

As PMMA and mPOFs are known for their water absorption [17, 18, 43]. A humidity test was done to understand how it might influence the FBG performance. Filling the vessel with distilled water with steps of 1 ml it is possible to determine the exact position of the FBG by the λ_{peak} shift and a height drop, presented in Fig. 3.2 (a) and (b) respectively. The resulting FBG spectra of the levels are presented in Fig. 3.3 (a), as the moisture level rises, the spectra of the main λ_{peak} FBG shifts $\sim +5\,nm$ due to a swell of the FBG [18].

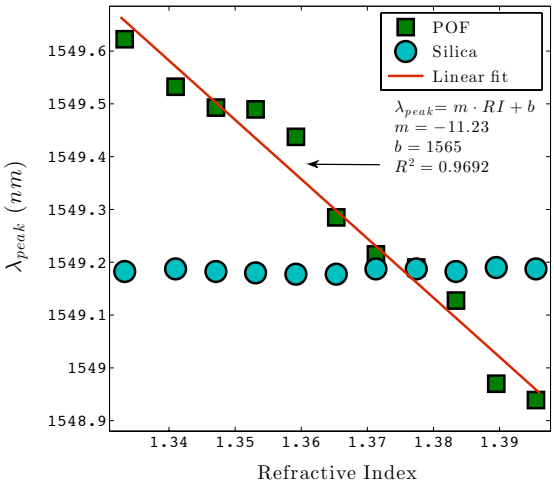

Figure 3.1: Influence of the glucose samples' RI on the PMMA and Silica fibres with no AOM.

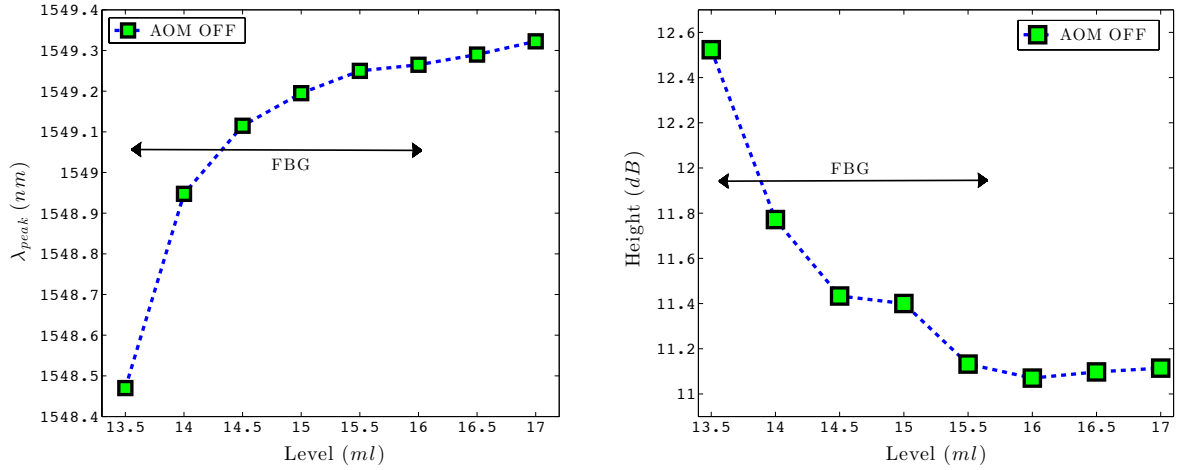

Figure 3.2: Variation of (a) λ_{peak} and (b) height of the peak, as the moisture diffuses inside the mPOF. The spectra stabilises at 16 ml, the level where the water fully covers the FBG.

The FBG absorption is a process where the moisture slowly diffuses into the fibre. As moisture diffuses, the cladding are filled with water resulting in an overlapping of the optical mode with the fluid [18]. It also increases the swell on grating. A moisture diffusing result is presented in Fig. 3.3 (b), where the spectra of FBG response at a level of 16 ml, completely covering the FBG. The result implies that before any measurement, the FBG must remain fully immersed in water for at least 90 min, ensuring spectral stability during the measurements.

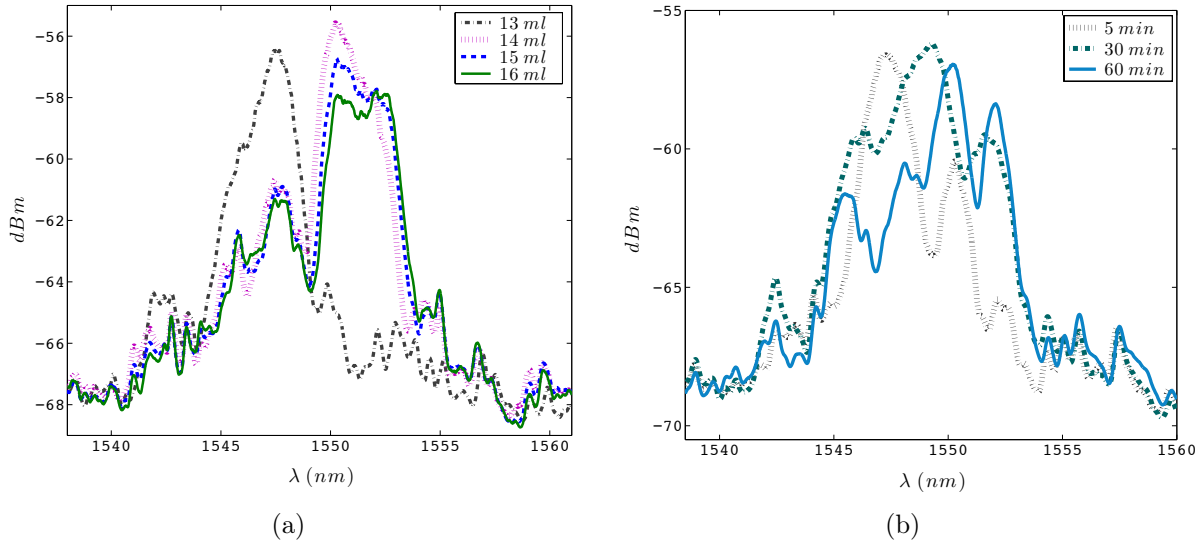

Figure 3.3: Spectra of the moisture test for mPOF, where (a) presents immersion at different levels; and (b) the moisture diffuse into the fibre as function of time for the 16 ml level.

3.2 Static

In this section, the results are processed to the difference between the AOM OFF and ON, further normalised to the measurable first value, discriminated for λ_{peak} as:

$$\frac{\Delta\lambda_{peak}(i)}{\Delta\lambda_{peak}(1)}, \quad \text{for} \quad \Delta\lambda_{peak} = \lambda_{AOM_{OFF}} - \lambda_{AOM_{ON}} \tag{3.1}$$

This normalisation is also applied for Bandwidth and Height data. In addiction, this normalisation is independent of the RI of the fluid under test, as the RI component is subtracted by $\Delta\lambda_{peak}$.

The calibration results for λ_{shift}, bandwidth and height for both mPOF and silica fibres are presented in Fig. 3.4 (a), (b) and (c) respectively. These results correspond to the 2^{nd} row of Tab. 3.2, where silica only presents viscosity correlation for bandwidth. The results for silica in term of λ_{shift} and height are displayed as well but not presenting a correlation. In term of bandwidth silica presents an exponential decay with the increase of viscosity, calibrated from 1.0837 to 5.0100 $mPa \cdot s$ with a bandwidth sensitivity of $-4.99\ \%/mPa \cdot s$ in respect to initial $\Delta Band.$.

The mPOF presents a exponential calibration for λ_{shift}, as seen is Fig. 3.4 (a). It discerns viscosity from 1.0837 to 1.9038 $mPa \cdot s$ achieving a blue shift sensitivity of $-94.42\ \%/mPa \cdot s$ in respect to initial $\Delta\lambda_{shift}$.

In terms of bandwidth and height on the mPOF, both correlate linearly with the increase of viscosity. The $Band._{norm}$ decreases with the increase of viscosity from 1.5600 to 4.2038 $mPa \cdot s$ with a sensitivity of $-4.95\ \%/mPa \cdot s$. The $Height_{norm}$ increases with the increase of viscosity from 1.5600 to 4.2038 $mPa \cdot s$, which represents an increase of the peak height achieving a sensitivity of $+2.50\ \%/mPa \cdot s$.

The experiment has shown that the shifting λ_{peak} present better calibration for pure flexural than hybrid modes. However for bandwidth and height, hybrid modes present higher correlation with viscosity. The appearance of hybrid acoustical modes, flexural plus longitudinal, are more common in the transitional region $\sim 400\ KHz$, as presented in Fig. 1.5. Hybrid modes contain a longitudinal component that creates a chirp on the grating, therefore for a fine tuning of the strain on the fibre, a stable phase matching is achieved. In this condition height and bandwidth present the linear correlation presented in Fig. 3.4. However in hybrid modes the longitudinal phase matching does not allow a correlation on λ_{shift}. Therefore the calibration of λ_{shift} presented in Fig. 3.4 (a) was done with a flexural mode ($f_a = 302.2\ KHz$), whereas both bandwidth and height with a hybrid mode ($f_a = 400\ KHz$), as seen in Fig. 3.4 (b) and (c) respectively.

Static results are summarised in terms of sensitivity in Tab. 3.3. Silica presents correlation for one of the three grating parameters tested, presenting an exponential decay of the bandwidth through the whole range of samples. For that same range on the mPOF, λ_{shift} covers the lower viscosity region ($1.0837 - 1.9038\ mPa \cdot s$) with a sensitivity of $-94.42\ \%/mPa \cdot s$, whereas bandwidth and height cover the higher viscosity region $1.5600 - 4.2038\ mPa \cdot s$.

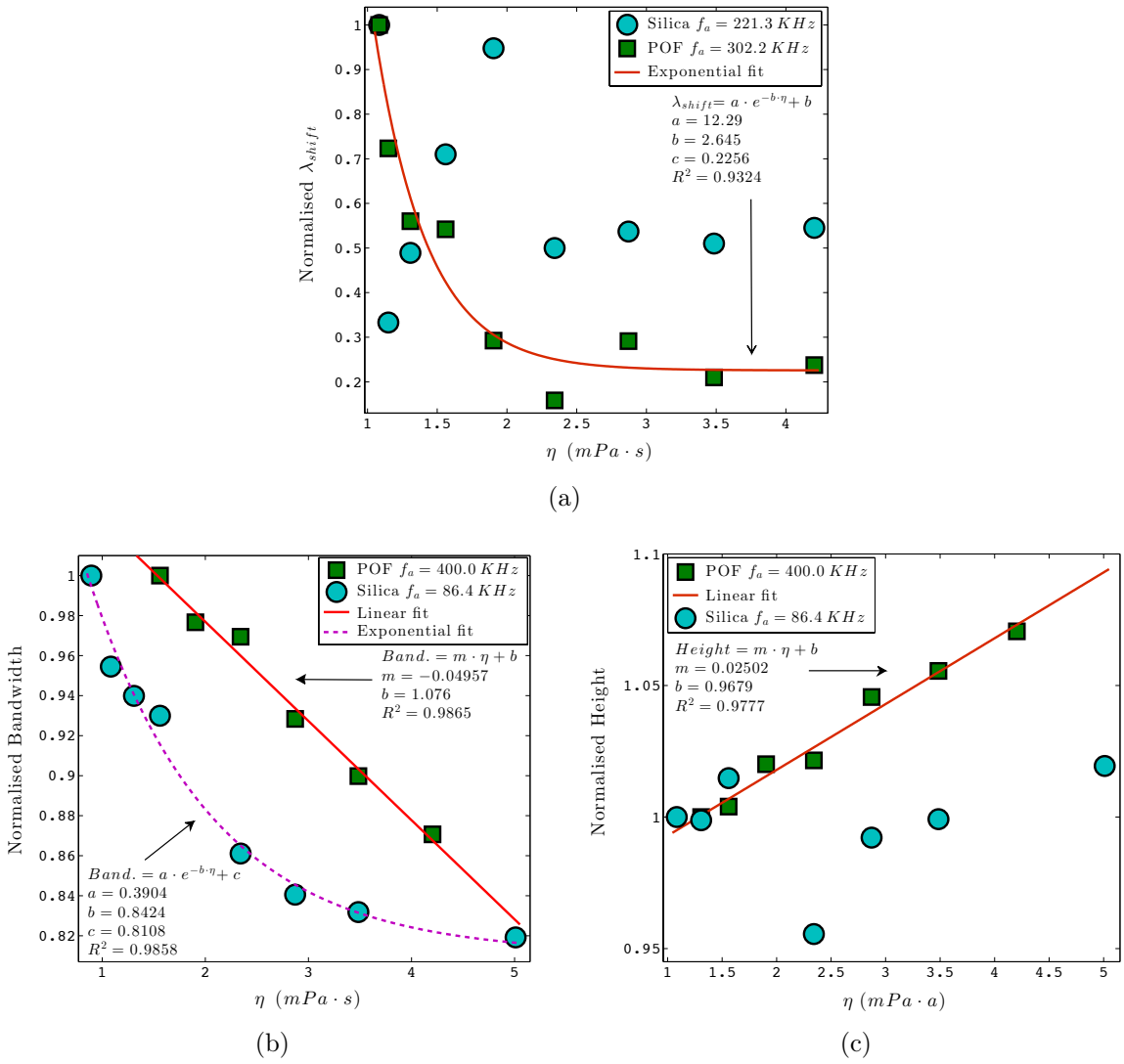

Figure 3.4: Calibration result of (a) λ_{shift}, (b) Bandwidth and (c) Height for glucose samples with mPOF and silica fibres. In (b) and (c) the results from the silica are displayed for comparison only. Data is normalised according to 3.1.

Table 3.3: Summary of viscosity range and sensitivity results for the static calibrations presented in Fig. 3.4.

	Calibration	$\eta\ (mPa \cdot s)$	Sensitivity $(\%/mPa \cdot s)$
mPOF	λ_{shift}	$1.0837 - 1.9038$	-94.42
	$Band.$	$1.5600 - 4.2038$	-4.95
	$Height$	$1.5600 - 4.2038$	$+2.50$
Silica	λ_{shift}	—	—
	$Band.$	$1.0837 - 5.0100$	-4.99
	$Height$	—	—

3.3 Dynamic

Introduced in section 2.4.2, the mPOF gratings do not present enough reflectivity to allow a clear dynamic measurement with the apparatus presented in Fig. 2.6 (a). In this apparatus, the photodiode can only resolve optical power $> -25\,dBm$. This limitation implies that our mPOFs grating cannot be detected, as they have peaks $< -50\,dBm$, as presented in Fig. 2.4 (a). Although, they were tested with erbium doped fibre amplifiers (EDFAs) amplification and a bandwidth filter, a typical time profile of the response is presented in Fig. 3.5. As the dynamic response of the mPOF presents a $SNR \sim 1$, it cannot be considered for measurements or calibrations, as the SNR is about one fifth of minimum acceptable for any physical measurement [40].

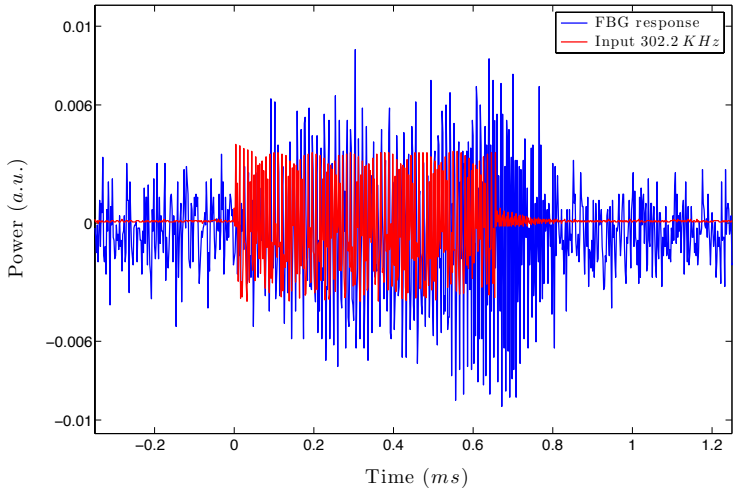

Figure 3.5: Typical dynamic response of a mPOF FBG under EDFA amplification on distilled water. As the $SNR \sim 1$ this calibration cannot be done. Note that the signal scales are adjusted for clear overview, as the input comes in V and the response in mV.

In this measurements it was avoided the use of flexural mode $f_a = 86.4\,KHz$ as it

saturates the photodiode, therefore two other flexural modes were selected: $f_a = 221.3\,KHz$ and $f_a = 227.0\,KHz$. The results for the decay time as a function of viscosity are presented in Fig. 3.6. The measurements show that the damping of the applied displacement is linear with viscosity. Linearity does correlates as expected from Eq. 1.4, where the drag force D is linear with the shear viscosity η.

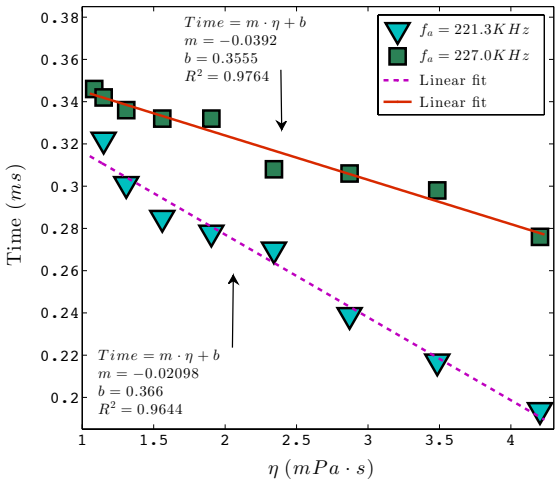

Figure 3.6: Decay times for two different flexural modes on a silica FBG. This corresponds to the apparatus presented in Fig. 2.6 (a).

For both frequencies the calibrations cover the viscosity samples analysed with a range $1.0837 - 5.0100\,mPa \cdot s$ presenting a sensitivity of $-0.039\,ms/mPa \cdot s$ for $f_a = 221.3\,KHz$, and $-0.020\,ms/mPa \cdot s$ for $f_a = 227.0\,KHz$. In Tab. 3.4 are summarised the sensitivities directly obtained by the linear fit and the normalised sensitivities with respect to fit parameter b.

Table 3.4: Summary of sensitivity results for the dynamic calibrations presented in Fig. 3.6.

Modes	Sensitivity $(ms/mPa \cdot s)$	Sensitivity $(\%/mPa \cdot s)$
$f_a = 221.3\,KHz$	-0.039	-10.98
$f_a = 227.0\,KHz$	-0.020	-5.36

In this work the decay is used instead of the rising and stabilisation times used by Oliveira *et al.* [3–5]. Despite that previous simulations predict a linear correlation between the rising and stabilisation times with the increase of viscosity assuming a constant force delivered by the PZT. Preliminary tests demonstrated an inconsistency of the rising and stabilisation times, found to be directly correlated with the complex impedance of PZT materials and their response to frequency excitation as studied by Kim [44]. Therefore, calibrations the rising and stabilisation times were invalidated due to a lack of control on current driven by the PZT.

Chapter 4

Conclusions

A prototype viscometer based on the AOM on FBGs was developed, characterised to RI and moisture absorption, and finally calibrated for viscosity measurements for both mPOF and silica fibres.

The design permits rapid interchange of samples, a clear view and access for its components, however it requires a pneumatic optical table for operation due to high sensitivity of whole system, especially working with mPOFs.

The AOM viscometer, based on static measurements is presented, comparing the mPOF and silica fibres performance. The highest sensitivity calibration was the mPOF, by combining the three grating parameters, λ_{shift}, height and bandwidth, achieving a maximum sensitivity of $-94.42\,\%/mPa \cdot s$ valid for a viscosity range of $1.0837 - 1.9038\,mPa \cdot s$. The achieved calibration demonstrated a greater flexibility for measurement with high sensitivity or wider range by only changing the operation frequency. The lower cost option of this sensor is the dynamic calibration using silica FBGs which minimises the cost of preparation and necessary equipment.

The net result from this work is a sensor that is closer to a possible commercial device, however the laboratory tests have demonstrated to be difficult to obtain a calibration through the preparation processes described. The reproducibility of the sensor is fairly low due to a lack of industrialised processes to equally fabricate two or more mPOF FBGs with optical connectors [16, 18]. However it is possible to use silica FBGs for dynamic measurements with cost benefits due to the available industrialised processes [12].

4.1 Future work

As with any work and any device, optimisation is one of paths to go further. Despite the issues already addressed and the problems contoured, many still remain that can be summarised in the measurements successful rate that is bellow 1 (e.g. the gauge ratio $^{successful}/_{failure}$). It means that more then 1 failure is need to get a successful measure, unbearable for a commercial device. This is also the opportunity to develop a new sensing mechanism that can avoid by design, as much as possible, the encountered issues.

4.1.1 Optimisation

The obtained results have shown that FBGs' reflectivity permits an higher degree for measurements and sensitivity. In particular, the mPOFs is limited to static tests only due to the low reflectivity. A possible way to overcome this limitation would be to use doped mPOF.

In the sensor system there are three big sources of problems: assemblage precision, humidity within the fibres and their connecting system.

Precision is ensured by the machined parts, but, the way these parts and optical components are assembled is not convenient resulting in mistakes. A better solution would be to pre-define dimensionality and machine the whole body from a solid block.

The humidity problem can be reduced using the TOPAS® polymer for the fibre instead of PMMA. It is known to reduce the moisture absorption by 30 times, therefore reducing the optical loss and achieving a stable FBG reflectivity spectra up to 90 % humidity [45]. However, using this fibre the sensor might loose the ability to discern RI as in the TOPAS fibre $\lambda_{shift} \sim 6\,pm$ from the minima to maximum moisture penetration [45], whereas in this work it was registered $\sim 5\,nm$. Nevertheless, for both PMMA and TOPAS based fibres, FBG should operate in the low loss optical visible wavelength as $\alpha = 1\,dB/m$ [18, 45].

The problem of connecting POF into silica fibre is the most difficult, as a proper industrialised and standardised cure is inexistent. The cure is a joint, a joint represents a weakness, to increase rigidity of the joint one have to choose harder materials for the joint. The NOA78 presents a RI of 1.50 and twice the viscosity of the NOA68 used [46, 47]. Higher viscosity represent easier handling of the adhesive, has in Fig. 2.3 (b), the adhesive tends to drip bellow the fibres due to gravity and bends the joint during the cure. Properties that would reduce the instabilities and optical losses on joint due to RI as the NOA78 RI is closer to the usual ~ 1.48 from PMMA at $1550\,nm$. Apart from a direct cure of a single mode mPOF into a single mode silica, it is also possible to do a taper, technique for reducing the fibre diameter by hot stretching, on a multi-mode silica fibre and then make with it on the mPOF.

Alternatively to curing process is to always use doped mPOF in order to achieve higher reflectivity. Thus it permits to have longer length of fibre after the bottom glued point, as indicated in Fig. 2.1, which allows to make optical connectors on the fibre tips, PC or APC, therefore reducing the loss on the interfaces and not suffering from the instabilities from the cure. Another possible solution is the use of a transitional waveguide between the mPOF and silica fibres, which might reduce the loss on the interface.

Combining the above proposals, it is expected to overcome the successful rate as mentioned, there is however, an uncertainty associated to the success of these implementations.

4.1.2 New Mechanism

In the initial objectives for this work, section 1.2, it was stated the intention to create a prototype viscometer that could be a possible low cost alternative to the today's available commercial devices. As the previous section proposes optimisations to improve the current

design, the design itself is still a mechanically sensible and does not offer integration into other systems. Nevertheless, the principle of operation relies too much on the grating characteristics which make it very difficult to produce two equal sensors, plus the associated cost for optical interrogation.

To address all these problems at once, a fundamental new design needs to be developed. One must go back to the initial step as presented in section 1.3.1 and find the root of how to relate all the components together assuming no boundaries. The current system can be discriminated by: acoustic-optic effect, fibre Bragg grating and viscosity. Fundamentally it uses the acoustic perturbation to *see* the viscosity outside, however acoustics waves don't actually interact directly with the fluid, instead they force the fibre to do just that, the grating is just the way for us, outside of the system, to detect differences.

The condition to measure viscosity is the damping of power or strain on the internal tensor of the fluid, as described by Eq. 1.3 and 1.4. In fact, taking a deep look to the equation, one can conclude that at the velocity v the drag D is linearly proportional, controlling the velocity and detecting the drag after a distance d, one might infer over the coefficient of shear stress viscosity η [33]. This principle indicates that it would more correct and simple to separate the the acoustic wave perturbation from the FBG detection system.

By placing the acoustic wave outside of the fibre and making it pass through the fluid, the velocity and strain of the wave will be damped by the shear stress, effect that can be detected by FBG. This idea is visually presented in Fig. 4.1 (a), where the cross section presents a tube wall with locus for both the PZT and optical fibre. The powerful enough PZT generates longitudinal acoustical waves, travelling through the sample and detected by the FBG. Fig. 4.1 (b) exhibit a perpendicular section view of the profile from Fig. 4.1 (a), the viscometer consists of a PZT and two independent FBGs.

In Fig. 4.2, a isometric rendering of the internal profile with displaying the locus for the active components dimensionality adjustment. The part itself enables integration of common pipe systems working as a buffer component.

Insulating the direct contract of the POF with the fluid with a thin rigid wall, all problems relating with humidity vanish, but, it also looses the refraction index ability. However a direct contact of the PZT with the structure of the tube will impart the perturbation to the FBG through the tube, an acoustic absorber must accommodate the PZT in place with an electrical insulated slot for the passage of the acoustic wave into the fluid.

The FBGs are supposed to operate in reflection, then using a photodiode, their spectra can be converted into a voltage signal, assuming the use of waveguides technic for the POF case as described in section 4.1.1. Therefore, the FBG will detect an incoming acoustic wave, that a powerful enough PZT, will decrease the FBG reflectivity, thus the observed signal. Two FBGs makes possible to detect the same acoustic signal twice, which under uniform and static fluid conditions can be correlated with viscosity and under moving fluid conditions, the power and phase shifts between the signals of FBGs can be correlated with velocity of the moving fluid, thus the flow.

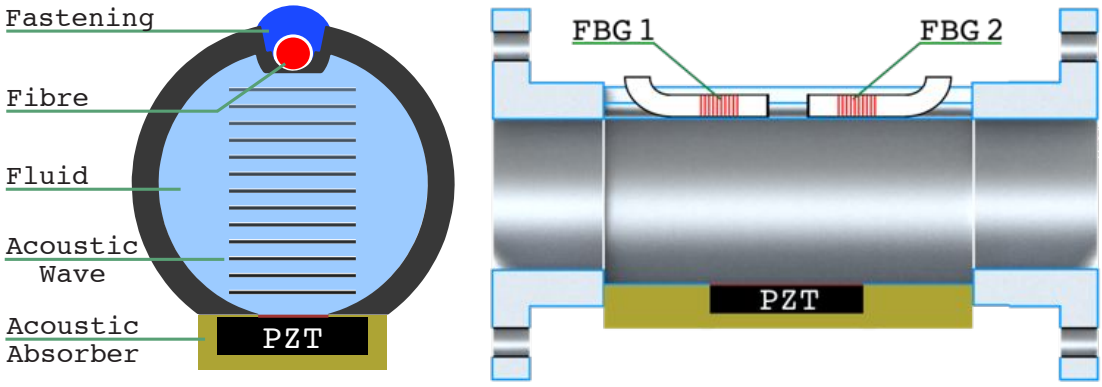

(a) (b)

Figure 4.1: In (a) profile illustration of the viscometer presenting the operation principle. In (b) a rendering of the section view along the axis, presenting the possible assembly position of the main sensing components for the viscometer. Dimensionality of the components is exaggerated for illustration purposes.

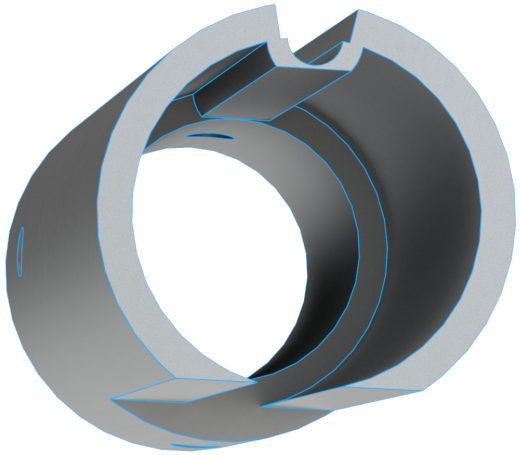

Figure 4.2: Isometric rendering of the proposed future viscometer sensor. The section view presents the internal cross section profile of the tube with the fibre accommodation on the top and PZT placement on the bottom.

This design, followed by proper calibration, should enable a sensor for viscosity featuring fluid direction and flow, flexible measurement range and integration on real systems providing the possibility for in-situ monitoring. Therefore, complementing the initials ambitions.

Bibliography

[1] J.Sapriel, *Acousto-Optics*. John Wiley & Sons, 1979.

[2] R. Oliveira, P. N. Jr., J. Pereira, and A. Pohl, "Numerical approach for designing a bragg grating acousto-optic modulator using the finite element and the transfer matrix methods," *Optics Communications*, vol. 281, no. 19, pp. 4899 – 4905, 2008.

[3] R. Oliveira, J. Canning, K. Cook, M. Nashqbandi, and A. Pohl, "Compact dip-style viscometer based on the acousto-optic effect in a long period fiber grating," *Sensors and Actuators B: Chemical*, vol. 157, no. 2, pp. 621 – 626, 2011.

[4] R. Oliveira, J. Canning, K. Cook, and A. A. P. Pohl, "Dip-style viscometer based on acoustic wave excitation of long period fibre grating," in *Optical Fibre Technology (ACOFT), 2010 35th Australian Conference on*, pp. 1–4, 2010.

[5] R. A. de Oliveira, *Characterization and new applications of the acousto-optic effect on fiber gratings*. PhD thesis, Federal University of Technology, Panará, Curitiba, 2011.

[6] A. Ramkumar and A. Lal, "Silicon ultrasonic horn actuated microprobes based self-calibrating viscosity sensor," in *Micro Electro Mechanical Systems (MEMS), 2010 IEEE 23rd International Conference on*, pp. 991–994, Jan. 2010.

[7] K. Sakai, T. Hirano, and M. Hosoda, "Electromagnetically spinning sphere viscometer," *Applied Physics Express*, vol. 3, no. 1, p. 016602, 2010.

[8] "Biophotonics and imaging conference." `http://www.bioopticsworld.com/articles/print/volume-6/issue-3/departments/news-notes/photoacoustics-microscopy--with-interdisciplinary-approach--biop.html`, 2013.

[9] K. Kao and G. Hockham, "Dielectric-fibre surface waveguides for optical frequencies," *IEE Proceedings*, vol. 133, no. 3, 1966.

[10] C. K. C. Menadier and H. Adkins, "The fotonic sensor," *I&CS- Control Technology Engineering*, vol. 40, pp. 114–114, 1967.

[11] G. Wild and S. Hinckley, "Acousto-ultrasonic optical fiber sensors: Overview and state-of-the-art," *Sensors Journal, IEEE*, vol. 8, no. 7, pp. 1184–1193, 2008.

[12] E. Udd, *Fiber Optic Sensors*. New York: Wiley, 1991.

[13] L. Bilro, N. Alberto, J. L. Pinto, and R. Nogueira, "Optical sensors based on plastic fibers," *Sensors*, vol. 12, no. 9, pp. 12184–12207, 2012.

[14] K. E. Carroll, C. Zhang, D. J. Webb, K. Kalli, A. Argyros, and M. C. Large, "Thermal response of bragg gratings in pmma microstructured optical fibers," *Opt. Express*, vol. 15, pp. 8844–8850, Jul 2007.

[15] J. C. Knight, T. A. Birks, P. S. J. Russell, and D. M. Atkin, "All-silica single-mode optical fiber with photonic crystal cladding," *Opt. Lett.*, vol. 21, pp. 1547–1549, Oct 1996.

[16] U. of Sidney, "Microstructured polymer optical fibre." `http://sydney.edu.au/ipos/research/groups/mpof.shtml`, Accessed: 18 July 2013.

[17] M. van Eijkelenborg, M. Large, A. Argyros, J. Zagari, S. Manos, N. Issa, I. Bassett, S. Fleming, R. McPhedran, C. M. de Sterke, and N. A. Nicorovici, "Microstructured polymer optical fibre," *Opt. Express*, vol. 9, pp. 319–327, Sep 2001.

[18] M. C. J. Large, D. Blacket, and C. A. Bunge, "Microstructured polymer optical fibers compared to conventional pof: Novel properties and applications," *Sensors Journal, IEEE*, vol. 10, no. 7, pp. 1213–1217, 2010.

[19] R. Kashyap, *Fiber Bragg Gratings*. Academic Press, 1999.

[20] F. Jülich and J. Roths, "Determination of the effective refractive index of various single mode fibres for fibre bragg grating sensor applications," in *SENSOR+TEST Conference*, (Nürnberg, Germany), 2009.

[21] H. Liu, G.-D. Peng, and P. Chu, "Polymer fiber bragg gratings with 28-db transmission rejection," *Photonics Technology Letters, IEEE*, vol. 14, no. 7, pp. 935–937, 2002.

[22] L. Brillouin, "Diffusion of light and x-rays by a transparent homogeneous body," *Ann. Phys.*, no. 17, pp. 88–122, 1922.

[23] F. S. P. Debye, "On the scattering of light by supersonic waves," *Proc. Nat. Acad. Sci. USA*, no. 6, pp. 409–414, 1932.

[24] "An anecdotal history of optics from aristophanes to zernike." `http://www.ee.umd.edu/~taylor/optics.htm`, Accessed: 2 June 2013.

[25] S. Inouye, S. Gupta, T. Rosenband, A. P. Chikkatur, A. Görlitz, T. L. Gustavson, A. E. Leanhardt, D. E. Pritchard, and W. Ketterle, "Observation of vortex phase singularities in bose-einstein condensates," *Phys. Rev. Lett.*, vol. 87, p. 080402, 2001.

[26] A. Korpel, "Acousto-optics - a review of fundamentals," *Proceedings of the IEEE*, vol. 69, no. 1, pp. 48–53, 1981.

[27] C. Marques, R. Oliveira, A. Pohl, J. Canning, and R. Nogueira, "Dynamic control of a phase-shifted fbg through acousto-optic modulation," *Optics Communications*, vol. 284, no. 5, pp. 1228 – 1231, 2011.

[28] A. Pohl, R. Oliveira, R. Silva, C. Marques, J. Neves, PaulodeTarso, K. Cook, J. Canning, and R. Nogueira, "Advances and new applications using the acousto-optic effect in optical fibers," *Photonic Sensors*, vol. 3, pp. 1–25, 2013.

[29] R. Oliveira, P. N. Jr., J. Pereira, J. Canning, and A. Pohl, "Vibration mode analysis of a silica horn-fiber bragg grating device," *Optics Communications*, vol. 283, no. 7, pp. 1296 – 1302, 2010.

[30] R. A. Oliveira, G. R. C. Possetti, C. A. F. Marques, P. T. N. Jr, K. Cook, R. C. Kamikawachi, C. Bavastri, J. L. Fabris, M. Muller, R. N. Nogueira, J. Canning, and A. A. P. Pohl, "Control of the long period grating spectrum through low frequency flexural acoustic waves," *Measurement Science and Technology*, vol. 22, no. 4, p. 045205, 2011.

[31] R. Oliveira, C. A. F. Marques, C. Mayer, J. Pereira, R. Nogueira, and A. Pohl, "Single device for excitation of both flexural and longitudinal acousto-optic effects in fiber bragg gratings," in *Microwave and Optoelectronics Conference (IMOC), 2009 SBMO/IEEE MTT-S International*, pp. 546–549, Nov. 2009.

[32] C. Marques, L. Bilro, L. Kahn, R. Oliveira, D. Webb, and R. Nogueira, "Acousto-optic effect in microstructured polymer fiber bragg gratings: Simulation and experimental overview," *Lightwave Technology, Journal of*, vol. 31, no. 10, pp. 1551–1558, 2013.

[33] B. Lautrup, *Physics of Continuous Matter: Exotic and Everyday Phenomena in the Macroscopic World*. Institute of Physics Publishing, 1 ed., 2005.

[34] J. Lighthill, *Waves in Fluids*. Cambridge University Press, 2001.

[35] Brookfield Engineering Laboratories, Inc., 11 Commerce Boulevard, Middleboro, MA 02346-1031 USA, *Brookfield Dial Reading Viscomter with Electronic Drive - Manual No. M/00-151*.

[36] P. C. Beard and T. N. Mills, "Extrinsic optical-fiber ultrasound sensor using a thin polymer film as a low-finesse fabry-perot interferometer," *Appl. Opt.*, vol. 35, pp. 663–675, Feb 1996.

[37] A. Stefani, W. Yuan, C. Markos, and O. Bang, "Narrow bandwidth 850-nm fiber bragg gratings in few-mode polymer optical fibers," *Photonics Technology Letters, IEEE*, vol. 23, no. 10, pp. 660–662, 2011.

[38] D. R. Lide, *CRC Handbook of Chemistry and Physics*. CRC Press, 2008.

[39] "Superfloc a-100." `http://www.hydrotechnik.org/SUPERFLOC_ASeries.pdf`, Accessed: 27 August 2013.

[40] D. Kong, J. Chang, P. Gong, Y. Liu, B. Sun, X. Liu, P. Wang, Z. Wang, W. Wang, and Y. Zhang, "Analysis and improvement of snr in fbg sensing system," *Photonic Sensors*, vol. 2, no. 2, pp. 148–157, 2012.

[41] X. Chen, C. Zhang, D. J. Webb, G.-D. Peng, and K. Kalli, "Bragg grating in a polymer optical fibre for strain, bend and temperature sensing," *Measurement Science and Technology*, vol. 21, no. 9, p. 094005, 2010.

[42] M. Unemori, Y. Matsuya, S. Matsuya, A. Akashi, and A. Akamine, "Water absorption of poly(methyl methacrylate) containing 4-methacryloxyethyl trimellitic anhydride," *Biomaterials*, vol. 24, no. 8, pp. 1381 – 1387, 2003.

[43] W. Zhang, D. Webb, and G. Peng, "Investigation into time response of polymer fiber bragg grating based humidity sensors," *Lightwave Technology, Journal of*, vol. 30, no. 8, pp. 1090–1096, 2012.

[44] H. Kim, *Impedance Adaptation Methods of the Piezoelectric Energy Harvesting.* `https://etda.libraries.psu.edu/paper/6979/`, The Pennsylvania State University, 2006.

[45] W. Yuan, L. Khan, D. J. Webb, K. Kalli, H. K. Rasmussen, A. Stefani, and O. Bang, "Humidity insensitive topas polymer fiber bragg grating sensor," *Opt. Express*, vol. 19, pp. 19731–19739, Sep 2011.

[46] "Noa68." `http://www.norlandprod.com/literature/68tds.pdf`.

[47] "Noa78." `https://www.norlandprod.com/literature/78tds.pdf`.

Appendix A

Spectra Data Analysis Code

Here are presented the *Matlab*® code for the developed program 'Spectra Data Analysis'. The graphical user interface file (*.fig*) is included in the delivered CD.

A.1 Main Program

```
function varargout = SpectraAnalysis(varargin)
% SPECTRAANALYSIS MATLAB code for SpectraAnalysis.fig
%       Ricardo Xavier Ferreira
%       ricardoxavier@ua.pt
%       Date: July 2013
%       Version: 3.1
%       This program is a companion to be used with spectra taken with the
%       Micron Optics - Optical Sensing Interrogator sm125.
%       It has a limitation that can only correctly treat 1 Peak per
%       Spetrum.
%       It has integrated plots of the Data Sets
%       It uses an external function to import the data files.
%       Further the peak are analised in dB witha -3dB drop for Bandwidth,
%       which corresponds to the FWHM.
% Last Modified by GUIDE v2.5 29-Jul-2013 00:53:07
gui_Singleton = 1;
gui_State = struct('gui_Name',       mfilename, ...
          'gui_Singleton',  gui_Singleton, ...
          'gui_OpeningFcn', @SpectraAnalysis_OpeningFcn, ...
          'gui_OutputFcn',  @SpectraAnalysis_OutputFcn, ...
          'gui_LayoutFcn',  [] , ...
          'gui_Callback',   []);
if nargin && ischar(varargin{1})
          gui_State.gui_Callback = str2func(varargin{1});
end
if nargout
          [varargout{1:nargout}] = gui_mainfcn(gui_State, varargin{:});
else
          gui_mainfcn(gui_State, varargin{:});
end
clc
end
```

```
33
34 function SpectraAnalysis_OpeningFcn(hObject, eventdata, handles, varargin)
35 handles.output = hObject;
36 guidata(hObject, handles);
37 xlabel(handles.Axes, ' Wavelength (nm) ','Interpreter','Tex','FontName','
       Courier','FontWeight','bold','FontSize',15);
38 ylabel(handles.Axes, ' Power (dBm) ','Interpreter','Tex','FontName','Courier
       ','FontWeight','bold','FontSize',15);
39 set(handles.Axes,'YMinorGrid','on','XMinorGrid','on','FontName','Courier','
       FontSize',13,'FontWeight','normal');
40 end
41
42 function varargout = SpectraAnalysis_OutputFcn(hObject, eventdata, handles)
43 varargout{1} = handles.output;
44 end
45
46 % ------------------------ My Code Starts Here ------------------------
47
48 function Spectrum1_Callback(hObject, eventdata, handles)
49 % Get channel info, store in channel panel Object 'UserData'
50 if      get(handles.CH1,'Value') == 1, CH.Spectrum1 = 1;
51 elseif get(handles.CH2,'Value') == 1, CH.Spectrum1 = 2;
52 elseif get(handles.CH3,'Value') == 1, CH.Spectrum1 = 3;
53 elseif get(handles.CH4,'Value') == 1, CH.Spectrum1 = 4;
54 end
55 set(handles.LCD,'String',sprintf('Importing on Channel %i ...',CH.Spectrum1)
       );
56 % Import file
57 Data = import_data(CH.Spectrum1);
58 UserData.Data = Data;
59 UserData.CH = CH.Spectrum1;
60 set(handles.Spectrum1,'UserData', UserData);
61 % Send Information to the user
62 set(handles.LCD,'String','Done');
63 guidata(hObject, handles); % Update Handles
64 end
65
66 function Spectrum2_Callback(hObject, eventdata, handles)
67 % Get channel info, store in channel panel Object 'UserData'
68 if      get(handles.CH1,'Value') == 1, CH.Spectrum2 = 1;
69 elseif get(handles.CH2,'Value') == 1, CH.Spectrum2 = 2;
70 elseif get(handles.CH3,'Value') == 1, CH.Spectrum2 = 3;
71 elseif get(handles.CH4,'Value') == 1, CH.Spectrum2 = 4;
72 end
73 set(handles.LCD,'String', sprintf('Importing on Channel %i ...',CH.Spectrum2
       ));
74 % Import file
75 Data = import_data( CH.Spectrum2 );
76 UserData.Data = Data;
77 UserData.CH = CH.Spectrum2;
78 set(handles.Spectrum2,'UserData', UserData);
79 % Send Information to the user
80 set(handles.LCD,'String','Done');
81 guidata(hObject, handles); % Update Handles
82 end
83
84 function Calculate_Callback(hObject, eventdata, handles)
85 clc  % Get the Data  and  Calculate: PeakPositon, FWHM, Height & Area.
```

```
% Spectrum 1
UserData = get(handles.Spectrum1,'UserData');
X1 = UserData.Data(:,1);
Y1 = UserData.Data(:,2);
clear UserData
% Spectrum 2
UserData = get(handles.Spectrum2,'UserData');
X2 = UserData.Data(:,1);
Y2 = UserData.Data(:,2);
clear UserData
% Smoothing
PopUp = get(handles.Smooth,'Value');
if PopUp == 1,
elseif PopUp == 2,                                          % POF
        Y1 = smooth(Y1,50,'moving');
        Y2 = smooth(Y2,50,'moving');
elseif PopUp == 3,                                          % Silica
        Y1 = smooth(Y1,9,'moving');
        Y2 = smooth(Y2,9,'moving');
else
end
% ---------- Calculate Spectra ----------
cla(handles.Axes);
set(handles.LCD,'String','Plotting...');
% Spectrum 1
plot(handles.Axes, X1, Y1,'-b'); % RAW data
% Spectrum 2
plot(handles.Axes, X2, Y2,'-m'); % RAW data
[y1, x1] = max(Y1);
y1Up=y1; x1Up=x1;
y1Down=y1; x1Down=x1;
i=1;
while y1Up(i)>(max(Y1)-3),    x1Up=(x1Up+1);       y1Up(i+1)=Y1(x1Up);       i=i
    +1; end
i=1;
while y1Down(i)>(max(Y1)-3), x1Down=(x1Down-1); y1Down(i+1)=Y1(x1Down); i=i
    +1; end
[y2, x2] = max(Y2);
y2Up   = y2; x2Up=x2;
y2Down = y2; x2Down=x2;
i=1;
while y2Up(i)>(max(Y2)-3),    x2Up=(x2Up+1);       y2Up(i+1)=Y2(x2Up);       i=i
    +1; end
i=1;
while y2Down(i)>(max(Y2)-3), x2Down=(x2Down-1); y2Down(i+1)=Y2(x2Down); i=i
    +1; end
clear x1 x2 y1 y2 i
FWHM1 = X1(x1Up) - X1(x1Down);
FWHM2 = X2(x2Up) - X2(x2Down);
% Calculate central Peak
PeakPosition1 = X1(x1Down) + (FWHM1 / 2);
PeakPosition2 = X2(x2Down) + (FWHM2 / 2);
Baseline1 = mean( [ Y1(1:x1Down); Y1(x1Up:end) ] ) ;
Baseline2 = mean( [ Y2(1:x2Down); Y2(x2Up:end) ] ) ;
XPeakPosition1 = round(x1Down + (x1Up - x1Down) /2);
XPeakPosition2 = round(x2Down + (x2Up - x2Down) /2);
% Calculate Height
```

```
Height1 = Y1(XPeakPosition1) - Baseline1;
Height2 = Y2(XPeakPosition2) - Baseline2;
% Calculate Integrated Area
Y1Linear = db2mag(Y1);
Y2Linear = db2mag(Y2);
Area1 = abs( db( abs( trapz(Y1Linear(x1Down:x1Up),X1(x1Down:x1Up)) ), 'power') ); % Intensity (a.u.)
Area2 = abs( db( abs( trapz(Y2Linear(x2Down:x2Up),X2(x2Down:x2Up)) ), 'power') ); % Intensity (a.u.)
% Sprectra Relative Diference (Percentage)
PeakPositionD = (PeakPosition1 - PeakPosition2);
FWHMD         = (FWHM2 ./ FWHM1);
HeightD       = (Height2 ./ Height1);
AreaD         = (Area2 ./ Area1);
% ---------- Calculate Spectra Data ----------
% Fit Spectrum 1
plot(handles.Axes,[PeakPosition1 PeakPosition1],[Baseline1 (Y1(round(XPeakPosition1))-0.05)],'-.','LineWidth',2,'Color',[0,0.3,0.5]); % Peak Position
plot(handles.Axes,[X1(x1Down) X1(x1Up)], [Y1(x1Down) Y1(x1Down)],'-.','LineWidth',2,'Color',[0,0.3,0.5]); % FWHM 1
plot(handles.Axes,[X1(x1Down+1) X1(x1Down+1)], [(Y1(x1Down)-0.3) (Y1(x1Down)+0.3)], '-','LineWidth',2,'Color',[0,0.3,0.5]); % FWHM 1
plot(handles.Axes,[X1(x1Up-1) X1(x1Up-1)], [(Y1(x1Down)-0.3) (Y1(x1Down)+0.3)], '-','LineWidth',2,'Color',[0,0.3,0.5]); % FWHM 1
% Fit Spectrum 2
plot(handles.Axes,[PeakPosition2 PeakPosition2],[Baseline2 (Y2(round(XPeakPosition2))-0.05)],'-.','LineWidth',2,'Color',[0.3,0,0.5]); % Peak Position
plot(handles.Axes,[X2(x2Down) X2(x2Up)], [Y2(x2Down) Y2(x2Down)],'-.','LineWidth',2,'Color',[0.3,0,0.5]); % FWHM 2
plot(handles.Axes,[X2(x2Down+1) X2(x2Down+1)], [(Y2(x2Down)-0.3) (Y2(x2Down)+0.3)], '-','LineWidth',2,'Color',[0.3,0,0.5]); % FWHM 2
plot(handles.Axes,[X2(x2Up-1) X2(x2Up-1)], [(Y2(x2Down)-0.3) (Y2(x2Down)+0.3)], '-','LineWidth',2,'Color',[0.3,0,0.5]); % FWHM 2
% Baseline
plot(handles.Axes,[X1(1) X1(end)],[Baseline1 Baseline1],'--','LineWidth',2,'Color',[0.5,0.5,0.5]);
% Truncate XX limits
if FWHM1 > FWHM2,
        Xm = (PeakPosition1 - ( 3*FWHM1 + 0) );
        XM = (PeakPosition1 + ( 3*FWHM1 + 0) );
else
        Xm = (PeakPosition2 - ( 3*FWHM2 + 0) );
        XM = (PeakPosition2 + ( 3*FWHM2 + 0) );
end
% Determine YY limits
if max(Y1) > max(Y2),
        YM = max(Y1) + 1;
        Ym = Baseline1 - 1.5;
else
        YM = max(Y2) + 1;
        Ym = Baseline2 - 1.5;
end
% ZOOM IN
axis(handles.Axes,[Xm XM Ym YM]);
```

```
% Set Box text alignment to the right
set(handles.PeakPosition1,'HorizontalAlignment','right');
set(handles.PeakPosition2,'HorizontalAlignment','right');
set(handles.FWHM1,'HorizontalAlignment','right');
set(handles.FWHM2,'HorizontalAlignment','right');
set(handles.Height1,'HorizontalAlignment','right');
set(handles.Height2,'HorizontalAlignment','right');
set(handles.PeakPositionD,'HorizontalAlignment','right');
set(handles.FWHMD,'HorizontalAlignment','right');
set(handles.HeightD,'HorizontalAlignment','right');
set(handles.Area1,'HorizontalAlignment','right');
set(handles.Area2,'HorizontalAlignment','right');
set(handles.AreaD,'HorizontalAlignment','right');
% Fill in boxes with the Values from Peaks and Differences
set(handles.PeakPosition1,'String', sprintf(' %0.4f ',PeakPosition1));
set(handles.PeakPosition2,'String', sprintf(' %0.4f ',PeakPosition2));
set(handles.FWHM1,'String',         sprintf(' %0.4f ',FWHM1));
set(handles.FWHM2,'String',         sprintf(' %0.4f ',FWHM2));
set(handles.Height1,'String',       sprintf(' %0.4f ',Height1));
set(handles.Height2,'String',       sprintf(' %0.4f ',Height2));
set(handles.PeakPositionD,'String', sprintf(' %0.4f ',PeakPositionD));
set(handles.FWHMD,'String',         sprintf(' %0.4f ',FWHMD));
set(handles.HeightD,'String',       sprintf(' %0.4f ',HeightD));
set(handles.Area1,'String',         sprintf(' %0.4f ',Area1));
set(handles.Area2,'String',         sprintf(' %0.4f ',Area2));
set(handles.AreaD,'String',         sprintf(' %0.4f ',AreaD));
% Send Information to the user
set(handles.LCD,'String','Done!');
guidata(hObject, handles); % Update Handles
end

function Append_Callback(hObject, eventdata, handles)
set(handles.LCD,'String','Appending...');
n = str2double(get(handles.AppendNumber,'String'));
% Get Previous Sets if they exist and Append
if n > 0; DataSet = get(handles.SpectraAnalysis,'UserData'); end
if isnan( str2double(get(handles.FWHM1,'String')) ),
        set(handles.LCD,'String','No Data to Append');
else
        PeakPosition1 = str2double(get(handles.PeakPosition1,'String'));
        FWHM1 = str2double(get(handles.FWHM1,'String'));
        Height1 = str2double(get(handles.Height1,'String'));
        Area1 = str2double(get(handles.Area1,'String'));
        PeakPosition2 = str2double(get(handles.PeakPosition2,'String'));
        FWHM2 = str2double(get(handles.FWHM2,'String'));
        Height2 = str2double(get(handles.Height2,'String'));
        Area2 = str2double(get(handles.Area2,'String'));
        PeakPositionD = str2double(get(handles.PeakPositionD,'String'));
        FWHMD = str2double(get(handles.FWHMD,'String'));
        HeightD = str2double(get(handles.HeightD,'String'));
        AreaD = str2double(get(handles.AreaD,'String'));
        % Construct DataSet Structure
        DataSet(n+1,1).PeakPosition1 = PeakPosition1;
        DataSet(n+1,1).PeakPosition2 = PeakPosition2;
        DataSet(n+1,1).PeakPositionD = PeakPositionD;
        DataSet(n+1,1).Height1 = Height1;
```

```
238             DataSet(n+1,1).Height2 = Height2;
239             DataSet(n+1,1).HeightD = HeightD;
240             DataSet(n+1,1).FWHM1 = FWHM1;
241             DataSet(n+1,1).FWHM2 = FWHM2;
242             DataSet(n+1,1).FWHMD = FWHMD;
243             DataSet(n+1,1).Area1 = Area1;
244             DataSet(n+1,1).Area2 = Area2;
245             DataSet(n+1,1).AreaD = AreaD;
246             % Send DataSet to handles
247             set(handles.SpectraAnalysis,'UserData',DataSet);
248             set(handles.AppendNumber,'String',num2str(n+1));
249             set(handles.LCD,'String','<< Appended >>');
250             % ZOOM out
251             axis(handles.Axes,[1510 1590 -70 0]);
252 end
253 end
254
255 function PlotSetRaw_Callback(hObject, eventdata, handles)
256 DataSet = get(handles.SpectraAnalysis,'UserData');
257 n = numel(DataSet);
258 for i=1:n,
259             Peak1(i) = DataSet(i).PeakPosition1;
260            FWHM1(i) = DataSet(i).FWHM1;
261             Height1(i) = DataSet(i).Height1;
262             Area1(i) = DataSet(i).Area1;
263             Peak2(i) = DataSet(i).PeakPosition2;
264            FWHM2(i) = DataSet(i).FWHM2;
265             Height2(i) = DataSet(i).Height2;
266             Area2(i) = DataSet(i).Area2;
267 end
268 figure(1);
269 set(1,'Color',[0.93 0.93 0.93]);
270 set(1,'Position',[60 60 800 600]);
271 x = linspace(1,n,n);
272 subplot(2,2,1);
273 plot(x,Peak1,'--bs','LineWidth',2,'MarkerEdgeColor','k','MarkerFaceColor','g
    ','MarkerSize',10); hold
274 plot(x,Peak2,'--ms','LineWidth',2,'MarkerEdgeColor','k','MarkerFaceColor','g
    ','MarkerSize',10);
275 xlabel(' Sample ','FontName','Arial','FontName','Monospaced','FontSize',16,'
    FontWeight','bold','Interpreter','Latex');
276 ylabel(' $\lambda_{peak}\:\:(nm)$ ','FontName','Monospaced','FontSize',16,'
    FontWeight','bold','Interpreter','Latex');
277 subplot(2,2,2);
278 plot(x,Height1,'--bs','LineWidth',2,'MarkerEdgeColor','k','MarkerFaceColor',
    'g','MarkerSize',10); hold
279 plot(x,Height2,'--ms','LineWidth',2,'MarkerEdgeColor','k','MarkerFaceColor',
    'g','MarkerSize',10);
280 xlabel(' Sample ','FontName','Monospaced','FontSize',16,'FontWeight','bold',
    'Interpreter','Latex');
281 ylabel(' $Height\:\:(dB)$ ','FontName','Monospaced','FontSize',16,'
    FontWeight','bold','Interpreter','Latex');
282 subplot(2,2,3);
283 plot(x,FWHM1,'--bs','LineWidth',2,'MarkerEdgeColor','k','MarkerFaceColor','g
    ','MarkerSize',10); hold
```

```
284 plot(x,FWHM2,'--ms','LineWidth',2,'MarkerEdgeColor','k','MarkerFaceColor','g
    ','MarkerSize',10);
285 xlabel(' Sample ','FontName','Monospaced','FontSize',16,'FontWeight','bold',
    'Interpreter','Latex');
286 ylabel(' $FWHM\:\:(nm)$ ','FontName','Monospaced','FontSize',16,'FontWeight'
    ,'bold','Interpreter','Latex');
287 subplot(2,2,4);
288 plot(x,Area1,'--bs','LineWidth',2,'MarkerEdgeColor','k','MarkerFaceColor','g
    ','MarkerSize',10); hold
289 plot(x,Area2,'--ms','LineWidth',2,'MarkerEdgeColor','k','MarkerFaceColor','g
    ','MarkerSize',10);
290 xlabel(' Sample ','FontName','Monospaced','FontSize',16,'FontWeight','bold',
    'Interpreter','Latex');
291 ylabel(' Intensity  (a.u.) ','FontName','Monospaced','FontSize',16,'
    FontWeight','bold','Interpreter','Latex');
292 end
293
294 function PlotSetNorm_Callback(hObject, eventdata, handles)
295 DataSet = get(handles.SpectraAnalysis,'UserData');
296 n = numel(DataSet);
297 for i=1:n,
298         DPeak(i) = DataSet(i).PeakPositionD;
299         DFWHM(i) = DataSet(i).FWHMD;
300         DHeight(i) = DataSet(i).HeightD;
301         DArea(i) = DataSet(i).AreaD;
302 end
303 x = linspace(1,n,n);
304 figure(2);
305 set(2,'Color',[0.75 0.75 0.75]);
306 set(2,'Position',[60 60 800 600]);
307 subplot(2,2,1);
308 plot(x,DPeak,'--ks','LineWidth',2,'MarkerEdgeColor','k','MarkerFaceColor','g
    ','MarkerSize',10);
309 xlabel(' Sample ','FontName','Arial','FontName','Monospaced','FontSize',16,'
    FontWeight','bold','Interpreter','Latex');
310 ylabel(' $\Delta\lambda_{peak}\:\:(nm)$ ','FontName','Monospaced','FontSize'
    ,16,'FontWeight','bold','Interpreter','Latex');
311 subplot(2,2,2);
312 plot(x,DHeight,'--ks','LineWidth',2,'MarkerEdgeColor','k','MarkerFaceColor',
    'g','MarkerSize',10);
313 xlabel(' Sample ','FontName','Monospaced','FontSize',16,'FontWeight','bold',
    'Interpreter','Latex');
314 ylabel(' Normalized Height ','FontName','Monospaced','FontSize',16,'
    FontWeight','bold','Interpreter','Latex');
315 subplot(2,2,3);
316 plot(x,DFWHM,'--ks','LineWidth',2,'MarkerEdgeColor','k','MarkerFaceColor','g
    ','MarkerSize',10);
317 xlabel(' Sample ','FontName','Monospaced','FontSize',16,'FontWeight','bold',
    'Interpreter','Latex');
318 ylabel(' Normalized FWHM ','FontName','Monospaced','FontSize',16,'FontWeight
    ','bold','Interpreter','Latex');
319 subplot(2,2,4);
320 plot(x,DArea,'--ks','LineWidth',2,'MarkerEdgeColor','k','MarkerFaceColor','g
    ','MarkerSize',10);
321 xlabel(' Sample ','FontName','Monospaced','FontSize',16,'FontWeight','bold',
    'Interpreter','Latex');
```

```
322 ylabel(' Normalized Intensity ','FontName','Monospaced','FontSize',16,'
    FontWeight','bold','Interpreter','Latex');
323 end
324
325 function SaveTXT_Callback(hObject, eventdata, handles)
326 n = str2double(get(handles.AppendNumber,'String'));
327 if n == 0,
328         % Get all data to SaveTXT
329         % Peak 1
330         Peak1 = get(handles.PeakPosition1,'String');
331         FWHM1 = get(handles.FWHM1,'String');
332         Height1 = get(handles.Height1,'String');
333         Area1 = get(handles.Area1,'String');
334         % Peak 2
335         Peak2 = get(handles.PeakPosition2,'String');
336         FWHM2 = get(handles.FWHM2,'String');
337         Height2 = get(handles.Height2,'String');
338         Area2 = get(handles.Area2,'String');
339         % Normalised: Peak 1 - Peak 2
340         PeakD = get(handles.PeakPositionD,'String');
341         FWHMD = get(handles.FWHMD,'String');
342         HeightD = get(handles.HeightD,'String');
343         AreaD = get(handles.AreaD,'String');
344         % Ask User for the file to write
345         set(handles.LCD,'String','Please choose a Directory and File Name');
346         [FileName, PathName] = uiputfile('*.txt','Save Peaks DataSet');
347         File = strcat(PathName,FileName);
348         % Write file with Titles: Channel, Peak Position, FWHM, Height, Area
349         set(handles.LCD,'String',sprintf('Writting to %s','File'));
350         % Writting each line to file
351         FID = fopen(File,'a+');
352         % Write current date and time
353         fprintf(FID,'File Name: %s \nCreation Date: %s \n\n', FileName,
                datestr(now));
354         % Write Header
355         fprintf(FID,'#Peak     Position(nm)     FWHM(nm)     Height(dB)
                Intensity(a.u.)\n');
356         % Write Peaks
357         fprintf(FID,'1        %s        %s        %s        %s \n', Peak1,
               FWHM1, Height1, Area1);
358         fprintf(FID,'2        %s        %s        %s        %s \n', Peak2,
               FWHM2, Height2, Area2);
359         fprintf(FID,'Norm     %s        %s        %s        %s \n \n \n',
               PeakD, FWHMD, HeightD, AreaD);
360         fclose(FID);
361         set(handles.LCD,'String',sprintf('File Saved as %s',FileName));
362 elseif n > 0,
363         % Get Appended DataSet to SaveTXT
364         DataSet = get(handles.SpectraAnalysis,'UserData');
365         % Ask User for the file to write
366         set(handles.LCD,'String','Please choose a Directory and File Name');
367         [FileName, PathName] = uiputfile({'*.txt';'*.mat'},'Save Peaks
                Parameters');
368         File = strcat(PathName,FileName);
369         % Write file with Titles: Channel, Peak Position, FWHM, Height, Area
370         set(handles.LCD,'String',sprintf('Writting to %s','File'));
```

```
371         % Writting each line to file
372         FID = fopen(File,'w'); % w > write, a+ > append to the end of file
373         % Write current date and time
374         fprintf(FID,'File Name: %s \nCreation Date: %s \n\n', FileName,
                datestr(now));
375         % Generate a Set of lines for each Pair of Spectra Calculated
376         for i = 1:1:n,
377                 % Write each Pair of the DataSet
378                 % Write Header
379                 fprintf(FID,'#Peak    Position(nm)    FWHM(nm)    Height(dB)
                        Intensity(a.u.)\n');
380                 % Write Peaks
381                 fprintf(FID,'1       %s        %s        %s        %s \n',
                    DataSet(i).PeakPosition1, DataSet(i).FWHM1, DataSet(i).
                    Height1, DataSet(i).Area1);
382                 fprintf(FID,'2       %s        %s        %s        %s \n',
                    DataSet(i).PeakPosition2, DataSet(i).FWHM2, DataSet(i).
                    Height2, DataSet(i).Area2);
383                 fprintf(FID,'Norm    %s        %s        %s        %s \n \n
                    \n', DataSet(i).PeakPositionD, DataSet(i).FWHMD, DataSet(
                    i).HeightD, DataSet(i).AreaD);
384         end
385         fclose(FID);
386
387         set(handles.LCD,'String',sprintf('File Saved as %s',FileName));
388 else
389         set(handles.LCD,'String','Unknown Error, no data was saved.');
390 end
391
392 guidata(hObject, handles); % Update Handles
393 end
394
395 function SaveMAT_Callback(hObject, eventdata, handles)
396 % Creates an .mat file with the DataSet
397 n = str2double(get(handles.AppendNumber,'String'));
398 if n == 0,
399         PeakPosition1 = str2double(get(handles.PeakPosition1,'String'));
400         FWHM1 = str2double(get(handles.FWHM1,'String'));
401         Height1 = str2double(get(handles.Height1,'String'));
402         Area1 = str2double(get(handles.Area1,'String'));
403         PeakPosition2 = str2double(get(handles.PeakPosition2,'String'));
404         FWHM2 = str2double(get(handles.FWHM2,'String'));
405         Height2 = str2double(get(handles.Height2,'String'));
406         Area2 = str2double(get(handles.Area2,'String'));
407         PeakPositionD = str2double(get(handles.PeakPositionD,'String'));
408         FWHMD = str2double(get(handles.FWHMD,'String'));
409         HeightD = str2double(get(handles.HeightD,'String'));
410         AreaD = str2double(get(handles.AreaD,'String'));
411         % Construct DataSet Structure
412         DataSet(n+1,1).PeakPosition1 = PeakPosition1;
413         DataSet(n+1,1).PeakPosition2 = PeakPosition2;
414         DataSet(n+1,1).PeakPositionD = PeakPositionD;
415         DataSet(n+1,1).Height1 = Height1;
416         DataSet(n+1,1).Height2 = Height2;
417         DataSet(n+1,1).HeightD = HeightD;
418         DataSet(n+1,1).FWHM1 = FWHM1;
419         DataSet(n+1,1).FWHM2 = FWHM2;
```

```
420             DataSet(n+1,1).FWHMD = FWHMD;
421             DataSet(n+1,1).Intensity1 = Area1;
422             DataSet(n+1,1).Intensity2 = Area2;
423             DataSet(n+1,1).IntensityD = AreaD;
424             uisave('DataSet','DataSingle');
425             set(handles.LCD,'String','File Saved');
426     elseif n > 0,
427             DataSet = get(handles.SpectraAnalysis,'UserData');
428             uisave('DataSet','DataSet');
429             set(handles.LCD,'String','File Saved');
430     end
431     end
432
433
434     function Reset_Callback(hObject, eventdata, handles)
435     % Cleaning
436     set(handles.LCD,'String', 'Cleaning' );
437     set(handles.Reset,'BackgroundColor',[0.7,1,0.5]);
438     clc;
439     cla(handles.Axes);
440     axis([1510  1590  -83  0]);
441     xlabel(handles.Axes,' Wavelength (nm) ','FontName','Courier','FontSize',15,'
            FontWeight','bold','Interpreter','Tex');
442     ylabel(handles.Axes,' Power (dBm) ','FontName','Courier','FontSize',15,'
            FontWeight','bold','Interpreter','Tex');
443     set(handles.Axes,'YMinorGrid','on','XMinorGrid','on','FontName','Courier','
            FontSize',13,'FontWeight','normal');
444     set(handles.SpectraAnalysis,'UserData',num2str([]));
445     set(handles.Spectrum1,'UserData','');
446     set(handles.Spectrum2,'UserData','');
447     set(handles.AppendNumber,'String',num2str(0));
448     % Show the user green boxes
449     set(handles.PeakPosition1,'String',num2str([]));
450     set(handles.FWHM1,'String',num2str([]));
451     set(handles.Height1,'String',num2str([]));
452     set(handles.Area1,'String',num2str([]));
453     set(handles.PeakPosition2,'String',num2str([]));
454     set(handles.FWHM2,'String',num2str([]));
455     set(handles.Height2,'String',num2str([]));
456     set(handles.Area2,'String',num2str([]));
457     set(handles.PeakPositionD,'String',num2str([]));
458     set(handles.FWHMD,'String',num2str([]));
459     set(handles.HeightD,'String',num2str([]));
460     set(handles.AreaD,'String',num2str([]));
461     % Put boxes into the original state
462     set(handles.PeakPosition1,'HorizontalAlignment','center');
463     set(handles.FWHM1,'HorizontalAlignment','center');
464     set(handles.Height1,'HorizontalAlignment','center');
465     set(handles.Area1,'HorizontalAlignment','center');
466     set(handles.PeakPosition2,'HorizontalAlignment','center');
467     set(handles.FWHM2,'HorizontalAlignment','center');
468     set(handles.Height2,'HorizontalAlignment','center');
469     set(handles.Area2,'HorizontalAlignment','center');
470     set(handles.PeakPositionD,'HorizontalAlignment','center');
471     set(handles.FWHMD,'HorizontalAlignment','center');
472     set(handles.HeightD,'HorizontalAlignment','center');
```

```
473 set(handles.AreaD,'HorizontalAlignment','center');
474 set(handles.PeakPosition1,'String','-');
475 set(handles.FWHM1,'String','-');
476 set(handles.Height1,'String','-');
477 set(handles.PeakPosition2,'String','-');
478 set(handles.FWHM2,'String','-');
479 set(handles.Height2,'String','-');
480 set(handles.PeakPositionD,'String','-');
481 set(handles.FWHMD,'String','-');
482 set(handles.HeightD,'String','-');
483 set(handles.Area1,'String','-');
484 set(handles.Area2,'String','-');
485 set(handles.AreaD,'String','-');
486 set(handles.CH1,'Value',1);
487 set(handles.Smooth,'Value',1);
488 pause(0.4);
489 set(handles.Reset,'BackgroundColor',[0.92,0.92,0.92]);
490
491 set(handles.LCD,'String', 'Select Channel >> Import Spectrum' );
492 guidata(hObject, handles); % Update Handles
493 end
494
495 % ---------------- Useless, but compulsory ----------------
496
497 function Smooth_Callback(hObject, eventdata, handles)
498 end
499
500 function Smooth_CreateFcn(hObject, eventdata, handles)
501 if ispc && isequal(get(hObject,'BackgroundColor'), get(0,'
      defaultUicontrolBackgroundColor'))
502         set(hObject,'BackgroundColor','white');
503 end
504 end
505
506 function SpectraAnalysis_CloseRequestFcn(hObject, eventdata, handles)
507 clear all
508 delete(SpectraAnalysis);
509 clear all
510 end
```

A.2 Data Import Function

```
1 function Data = import_data(channel) % Header can be added as [Data Headers]
2 % Get File Name and Path
3 [fileName, pathName] = uigetfile({'*.txt;*.csv;*.dat;*.asc;*.ascii';'*.*'},'
    Pick Text File');
4 % Concatenates Path with File Name
5 file = strcat(pathName,fileName);
6 importedData = importdata(file);
7 Data = importedData.data(:,1);                    % Wavelength
8 Data(:,2) = importedData.data(:, channel+1);      % Channel used
9 end
```